Synthetic stellar photometry – I. General considerations and new transformations for broad-band systems

L. Casagrande[1][★][†] and Don A. VandenBerg[2]

[1]*Research School of Astronomy and Astrophysics, Mount Stromlo Observatory, The Australian National University, ACT 2611, Australia*
[2]*Department of Physics & Astronomy, University of Victoria, PO Box 1700 STN CSC, Victoria, BC V8W 2Y2, Canada*

ABSTRACT

After a pedagogical introduction to the main concepts of synthetic photometry, colours and bolometric corrections in the Johnson–Cousins, 2MASS, and *HST*-ACS/WFC3 photometric systems are generated from MARCS synthetic fluxes for various [Fe/H] and [α/Fe] combinations, and virtually any value of $E(B - V) \lesssim 0.7$. The successes and failures of model fluxes in reproducing the observed magnitudes are highlighted. Overall, extant synthetic fluxes predict quite realistic broad-band colours and bolometric corrections, especially at optical and longer wavelengths: further improvements of the predictions for the blue and ultraviolet spectral regions await the use of hydrodynamic models where the microturbulent velocity is not treated as a free parameter. We show how the morphology of the colour–magnitude diagram (CMD) changes for different values of [Fe/H] and [α/Fe]; in particular, how suitable colour combinations can easily discriminate between red giant branch and lower main-sequence populations with different [α/Fe], due to the concomitant loops and swings in the CMD. We also provide computer programs to produce tables of synthetic bolometric corrections as well as routines to interpolate in them. These colour–$T_{\rm eff}$–metallicity relations may be used to convert isochrones for different chemical compositions to various bandpasses assuming observed reddening values, thus bypassing the standard assumption of a constant colour excess for stars of different spectral type. We also show how such an assumption can lead to significant systematic errors. The MARCS transformations presented in this study promise to provide important constraints on our understanding of the multiple stellar populations found in globular clusters (e.g. the colours of lower main-sequence stars are predicted to depend strongly on [α/Fe]) and of those located towards/in the Galactic bulge.

Key words: techniques: photometric – stars: atmospheres – stars: fundamental parameters – Hertzsprung–Russell and colour–magnitude diagrams – globular clusters: general.

1 INTRODUCTION

Photometric systems and filters are designed to be sensitive to temperature, gravity, or metal abundance indicators and thereby to complement spectroscopic determinations of the fundamental properties of stars. Moreover, when studying more complex systems such as star clusters and galaxies, the integrated magnitudes and colours of stars can be used to infer the ages, metallicities, and other properties of the underlying stellar populations. To accomplish this, filter systems are tailored to select regions in stellar spectra where the variations of the atmospheric parameters leave their characteristic traces with enough prominence to be detected in photometric data. Begin-

ning with the influential papers by Johnson (1966) and Strömgren (1966), which describe the basis of broad- and intermediate-band photometry, a large number of systems exists nowadays, and more are being developed with the advent of extensive photometric surveys (see e.g. Bessell 2005, for a review).

Broad-band colours are usually tightly correlated with the stellar effective temperature ($T_{\rm eff}$), although metallicity ([Fe/H]) and (to a lesser extent) surface gravity ($\log g$) also play a role, especially towards the near-ultraviolet (UV) and the Balmer discontinuity (e.g. Eggen, Lynden-Bell & Sandage 1962; Ridgway et al. 1980; Bell & Gustafsson 1989; Alonso, Arribas & Martinez-Roger 1996; Ivezić et al. 2008; Casagrande et al. 2010). On the other hand, intermediate- and/or narrow-band filters centred on specific spectral features can have a much higher sensitivity to stellar parameters other than $T_{\rm eff}$ (e.g. Strömgren 1966; Wing 1967; McClure & van den Bergh 1968; Golay 1972; Mould & Siegel 1982; Worthey et al. 1994). While

[★]E-mail: luca.casagrande@anu.edu
[†]Stromlo Fellow.

broad-band photometry can be easily used to map and study extended stellar populations and/or large fractions of the sky, also at faint magnitudes (e.g. Stetson, Hesser & Smecker-Hane 1998; Bedin et al. 2004; Ivezić et al. 2007; Saito et al. 2012), intermediate- and narrow-band photometry is more limited in this respect, although still very informative (e.g. Bonnell & Bell 1982; Mould & Bessell 1982; Yong et al. 2008; Árnadóttir, Feltzing & Lundström 2010; Casagrande et al. 2014b).

In principle, determining stellar parameters from photometric data is a basic task, yet empirical calibrations connecting them are generally limited to certain spectral types and/or involve substantial observational work. In recent years, we have made a considerable effort to derive empirical relations that link photometric indices to the effective temperatures and metallicities of dwarf and subgiant stars (Casagrande et al. 2010, 2011). In particular, our studies of solar twins have enabled us to accurately set the zero-points of both the [Fe/H] and $T_{\rm eff}$ scales for the first time (Meléndez et al. 2010; Casagrande et al. 2012; Ramírez et al. 2012, similar work is currently underway for giants, see also Casagrande et al. 2014a). The zero-point of photometrically derived $T_{\rm eff}$ is also intimately connected to the absolute calibration of photometric systems; i.e. it is crucial to convert magnitudes into fluxes and vice versa, be they synthetic or observed.

Parallel to this empirical approach, in the spirit of VandenBerg & Clem (2003) and Clem et al. (2004), we have also tested the performance of synthetic colours against field and cluster stars of different evolutionary stages (Brasseur et al. 2010; VandenBerg, Casagrande & Stetson 2010). Such comparisons, which have been carried out using the Victoria-Regina models (VandenBerg et al. 2012) and an initial set of colour transformations based on one-dimensional MARCS synthetic stellar fluxes (Gustafsson et al. 2008), have validated the accuracy of the adopted library in predicting broad-band colours for a wide range of $T_{\rm eff}$ and [Fe/H] relevant to dwarf stars and subgiants. Some discrepancies between the predicted and observed colours of giants were found, but they could be telling us that the model temperatures are not realistic because of deficiencies in, e.g. the treatment of convection or the atmospheric boundary condition. It is also possible that these differences stem from abundance anomalies in some of the globular clusters that were used in these studies.

In this paper, we continue our efforts to provide reliable MARCS synthetic colours for different [Fe/H] and [α/Fe] combinations in the most commonly used optical and infrared (IR) photometric systems (Fig. 1). In particular, we take full advantage of the accuracy we have established concerning the absolute calibration of photometric systems to compute synthetic colours with well-defined zero-points. Also, for the first time, we generate synthetic colours accounting for different values of the reddening, $E(B-V)$, thus bypassing the usual assumption that the colour excess is independent of spectral type. Our purpose here is thus twofold: together with assessing the performance of the latest MARCS grids of synthetic fluxes in different bands, we provide several computer programs (in FORTRAN) to produce, and interpolate in, tables of bolometric corrections (BCs, see Appendix A). The resultant colour–$T_{\rm eff}$–metallicity relations are given for the most commonly used broad-band systems.

2 SYNTHETIC PHOTOMETRY

The basic idea of synthetic photometry is to reproduce observed colours (be they stars, planets, or galaxies) based simply on input (usually theoretical) spectra f_x, and a characterization of the instrumental system response function T_ζ under which the photo-
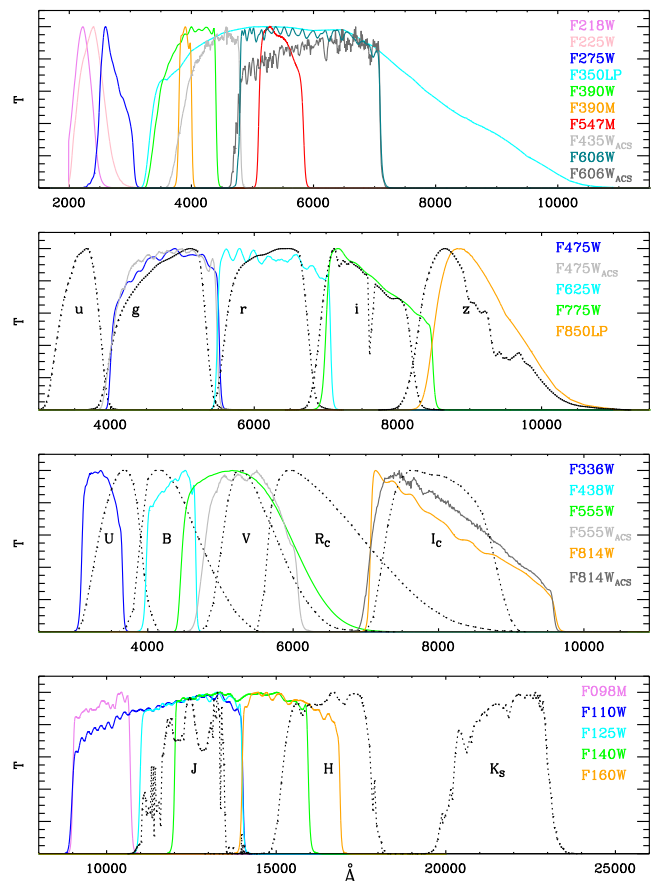

Figure 1. System response functions from which synthetic colours have been computed. All curves are normalized to one, and shown in arbitrary units as function of wavelength (in Å). For the *HST* system, different colours correspond to the names on the right-hand side of each panel (WFC3, unless the subscript indicates the ACS camera). Sloan (second), Johnson–Cousins (third) and 2MASS (fourth panel) system response functions are plotted with dotted lines and the name of each filter is indicated next to its curve. Some of the *HST* filters are designed to broadly match the Sloan and Johnson–Cousins systems: compare dotted and continuous lines in the second and third panel.

metric observations are performed (i.e. the total throughput of the optics, detector, filter, etc., over a spectral range x_A–x_B. If observations are ground based, then the atmospheric transmission must also be included in the throughput: this is often done at a nominal airmass of 1.3). Thus, in its most general and simplest form, a synthetic magnitude can be written as proportional (via a logarithmic factor, see Section 2.1) to $\int_{x_A}^{x_B} f_x\,T_\zeta\,{\rm d}x$, where the integration over x is carried out either in wavelength or frequency space. This relation also highlights the fact that a magnitude can be simply thought of as an heterochromatic measurement, where the information encoded in the spectrum is weighted by T_ζ.[1] Depending on the spectral coverage and the transmissivity of T_ζ, the result will depend more or less strongly upon (some of) the physical parameters of the underlying spectrum. By employing different filter combinations, it is then possible to highlight certain spectral features. If

---

[1] Because synthetic magnitudes are essentially a weighted average of the flux, the correct formalism requires a normalization over T_ζ, thus $\frac{\int_{x_A}^{x_B} f_x\,T_\zeta\,{\rm d}x}{\int_{x_A}^{x_B} T_\zeta\,{\rm d}x}$.

we are interested in stellar colours, these could be, for instance, the slope of the continuum, the depression owing to metal lines, the Balmer discontinuity, etc. which in turn tell us about the basic stellar parameters.

The advantage of using synthetic libraries is that they cover uniformly and homogeneously a range of stellar parameters – a feature which is appealing for a number of reasons including, in particular, the transposition of theoretical stellar models from the $T_{\rm eff}$–luminosity plane on to the observational colour–magnitude diagram (CMD). Several papers deal with this topic, and excellent discussions on synthetic photometry can be found in e.g. Bessell, Castelli & Plez (1998), Girardi et al. (2002), and Bessell & Murphy (2012).

2.1 From fluxes to magnitudes

Even though the physical quantities that we work with are fluxes, in astronomy it is customary to deal with magnitudes, a concept that is thought to have originated with Hipparchus. In his system, the brightest stars in the sky, first magnitude, were considered to be about twice as bright as those of second magnitude, and so forth until the faintest stars visible with the naked eye, which are about one hundred times fainter, were classified as sixth magnitude. This concept was formalized by Pogson (1856), who conveniently proposed that a first magnitude star be $100^{1/5} \simeq 2.5$ times as bright as a second magnitude star. This underpins the *definition* of magnitudes as proportional to $-2.5 \log$ of the flux, i.e.

$$m_1 - m_2 = -2.5 \log \frac{\int_{x_A}^{x_B} f_{x,1}\, T_\zeta\, {\rm d}x}{\int_{x_A}^{x_B} f_{x,2}\, T_\zeta\, {\rm d}x}, \tag{1}$$

where in the case of Pogson T_ζ was the transmission of the eye, and using m_2 and $f_{x,2}$ as standard star (or the Hipparchus 'first magnitude stars'), the heterochromatic definition of a photometric system is readily obtained (see e.g. equation 8). The fact that a non-linear transformation relates magnitudes to fluxes, is a potential source of bias, which we deal with in Appendix B. Here, it suffices to mention that this bias arises when using poor-quality data, and assuming that Gaussian random errors in fluxes are mapped into Gaussian random errors in magnitudes, and vice versa.

2.2 Photon counting versus energy integration

Before dealing with specific magnitude systems, one further concept must be introduced. The system response function T_ζ represents the total throughput in reaching the observer, which is affected by everything lying between a photon as it arrives at the top of the Earth's atmosphere and its final detection (e.g. Golay 1974). A proper characterization of T_ζ is therefore non-trivial, although nowadays it is accurately known for most photometric systems. Among the different stages and components which define the total throughput, the most important ones are arguably the filter itself and the response function of the detector. The latter must be taken into account in the response function of the overall system because, in all instances, the flux is evaluated after entering the detector. Because of this, one must distinguish between photon-counting (e.g. CCD) and energy-integration (e.g. photomultiplier) detectors (e.g. Bessell 2000; Maíz Apellániz 2006; Bessell & Murphy 2012).

For a CCD system, the rate of arrival of photons (number per unit time per detector area) from a source having a flux f_λ is $\int \frac{f_\lambda}{h\nu}\, T_\zeta\, {\rm d}\lambda$, while the energy measured in the same window of time over the same detector area is simply $\int f_\lambda T_\zeta\, {\rm d}\lambda$. Since a CCD counts pho-

tons (or actually converts photons into electrons with a given efficiency), it follows that $\int \frac{f_\lambda}{h\nu}\, T_\zeta\, {\rm d}\lambda = \frac{1}{hc} \int f_\lambda\, \lambda\, T_\zeta\, {\rm d}\lambda$; i.e. the energy formalism can also be used for a CCD, if T_ζ is replaced by $\lambda\, T_\zeta$ (or equivalently, T_ζ by $\frac{T_\zeta}{\nu}$ if working in frequency space). A common source of confusion when using published response functions for different photometric systems is whether or not T_ζ has already been multiplied by λ. Throughout this paper, the formalism that we introduce for heterochromatic measurements always assumes that T_ζ is provided in energy integration form and that all synthetic colours are generated for photon-counting systems; i.e. we explicitly introduce the $\lambda\, T_\zeta$ (or $\frac{T_\zeta}{\nu}$) term in the equations of synthetic photometry. (Note that the hc constant disappears because of the normalization over T_ζ). Since energy integration response functions are the correct ones to use in the photon-counting formalism, they are sometimes also called photonic response functions (e.g. Bessell & Murphy 2012). Among the existing photometric packages, the most commonly used one is SYNPHOT (Laidler et al. 2008), which comply with the photon-counting formalism (and photonic response functions) described here.[2] Needless to say, in a number of cases where the published values of T_ζ already include the λ dependence (see Table 1), the photon-counting synthetic quantities have been calculated using the energy-integration formalism.

2.3 ST mag system

ST monochromatic magnitudes (i.e. per unit wavelength) are defined as

$$m_{\rm ST} = -2.5 \log f_\lambda + ZP_\lambda, \tag{2}$$

where, by construction, a constant flux density per unit wavelength $f_\lambda^0 = 3.631 \times 10^{-9}\, {\rm erg\, s^{-1}\, cm^{-2}\, \mathring{A}^{-1}}$ is defined to have $m_{\rm ST} = 0.0$, thus implying $ZP_\lambda = -21.10$. Since in reality all measurements are heterochromatic, it follows that ST magnitudes are in fact defined over the wavelength range λ_i to λ_f which characterizes a given bandpass ζ that has a system response function T_ζ

$$m_{\rm ST} = -2.5 \log \frac{\int_{\lambda_i}^{\lambda_f} \lambda f_\lambda T_\zeta\, {\rm d}\lambda}{\int_{\lambda_i}^{\lambda_f} \lambda T_\zeta\, {\rm d}\lambda} - 21.10 = -2.5 \log \frac{\int_{\lambda_i}^{\lambda_f} \lambda f_\lambda T_\zeta\, {\rm d}\lambda}{f_\lambda^0 \int_{\lambda_i}^{\lambda_f} \lambda T_\zeta\, {\rm d}\lambda}. \tag{3}$$

To express the above λ-formalism in terms of a constant flux density per unit frequency, the only change that needs to be made to equation (3) is to replace f_λ^0 by $f_\nu^0 \frac{c}{\lambda^2}$.

2.4 AB mag system

Conceptually identical to the ST magnitudes, the AB system is defined as

$$m_{\rm AB} = -2.5 \log f_\nu + ZP_\nu, \tag{4}$$

where, in this case, $m_{\rm AB} = 0.0$ corresponds to a constant flux density per unit frequency $f_\nu^0 = 3.631 \times 10^{-20}\, {\rm erg\, s^{-1}\, cm^{-2}\, Hz^{-1}}$, thus implying $ZP_\nu = -48.60$. Integrating over frequencies (heterochromatic measurement)

$$m_{\rm AB} = -2.5 \log \frac{\int_{\nu_i}^{\nu_f} f_\nu \frac{T_\zeta}{\nu}\, {\rm d}\nu}{\int_{\nu_i}^{\nu_f} \frac{T_\zeta}{\nu}\, {\rm d}\nu} - 48.60 = -2.5 \log \frac{\int_{\nu_i}^{\nu_f} f_\nu T_\zeta\, {\rm d}\ln\nu}{f_\nu^0 \int_{\nu_i}^{\nu_f} T_\zeta\, {\rm d}\ln\nu} \tag{5}$$

---

[2] http://www.stsci.edu/institute/software_hardware/stsdas/synphot and its python version http://stsdas.stsci.edu/pysynphot

Table 1. Characteristic parameters defining the photometric systems studied here. The absolute calibration $\bar{f}_{\star,\zeta}$ (obtained using a spectrum of Vega as defined in Section 2.5) is given in $\mathrm{erg\,s^{-1}\,cm^{-2}\,\text{Å}^{-1}}$.

Filter	T_ζ	VEGA system			AB system	ST system
		$m_{*,\zeta}$	$\bar{f}_{\star,\zeta}$	ϵ_ζ	ϵ_ζ	ϵ_ζ
UX	1*	+0.020	4.0275E-9	0	–	–
BX	1*	+0.020	6.2712E-9	0	–	–
B	1*	+0.020	6.3170E-9	0	–	–
V	1*	+0.030	3.6186E-9	0	–	–
R_C	1*	+0.039	2.1652E-9	0	–	–
I_C	1*	+0.035	1.1327E-9	0	–	–
U	2	–	–	–	−0.761	–
B	2	–	–	–	+0.130	–
V	2	–	–	–	+0.020	–
R_C	2	–	–	–	−0.163	–
I_C	2	–	–	–	−0.404	–
J	3*	−0.001	3.129E-10	−0.017	–	–
H	3*	+0.019	1.133E-10	+0.016	–	–
K_S	3*	−0.017	4.283e-11	+0.003	–	–
u	4	–	–	–	+0.037	–
g	4	–	–	–	−0.010	–
r	4	–	–	–	+0.003	–
i	4	–	–	–	−0.006	–
z	4	–	–	–	−0.016	–
$F435W_{\mathrm{ACS}}$	5	0	6.4530E-9	0	0	0
$F475W_{\mathrm{ACS}}$	5	0	5.3128E-9	0	0	0
$F555W_{\mathrm{ACS}}$	5	0	3.8191E-9	0	0	0
$F606W_{\mathrm{ACS}}$	5	0	2.8705E-9	0	0	0
$F814W_{\mathrm{ACS}}$	5	0	1.1353E-9	0	0	0
$F218W$	6	0	4.6170E-9	0	0	0
$F225W$	6	0	4.1887E-9	0	0	0
$F275W$	6	0	3.7273E-9	0	0	0
$F336W$	6	0	3.2449E-9	0	0	0
$F350LP$	6	0	2.7464E-9	0	0	0
$F390M$	6	0	6.5403E-9	0	0	0
$F390W$	6	0	5.7932E-9	0	0	0
$F438W$	6	0	6.6896E-9	0	0	0
$F475W$	6	0	5.2240E-9	0	0	0
$F547M$	6	0	3.6694E-9	0	0	0
$F555W$	6	0	3.9511E-9	0	0	0
$F606W$	6	0	2.9094E-9	0	0	0
$F625W$	6	0	2.4383E-9	0	0	0
$F775W$	6	0	1.3104E-9	0	0	0
$F814W$	6	0	1.1486E-9	0	0	0
$F850LP$	6	0	8.0146E-10	0	0	0
$F098M$	6	0	6.6687E-10	0	0	0
$F110W$	6	0	4.0648E-10	0	0	0
$F125W$	6	0	3.0448E-10	0	0	0
$F140W$	6	0	2.0837E-10	0	0	0
$F160W$	6	0	1.4553E-10	0	0	0

Note: An asterisk in the second column indicates that T_ζ given in the reference is already multiplied by λ and renormalized. 1: Bessell (1990). 2: Bessell & Murphy (2012): notice that the formalism introduced in that paper for the $UBV(RI)_C$ system is in terms of AB magnitudes, although the system is actually VEGA based; ϵ_ζ values are obtained from their tables 3 and 5 (but with the opposite sign, following our definition of ϵ_ζ). 3: Cohen et al. (2003); ϵ_ζ values from Casagrande et al. (2010). 4: SDSS website; ϵ_ζ values are obtained comparing the observed magnitudes of a number of *HST* CALSPEC standards with the magnitudes generated in the AB system using the adopted T_ζ with the *HST* absolute spectrophotometry. 5: http://www.stsci.edu/hst/acs/analysis/zeropoints. 6: http://www.stsci.edu/~WFC3/UVIS/SystemThroughput.

which is identical to, e.g. the photon-counting definition given by Fukugita et al. (1996). Recasting equation (5) in terms of wavelength results in

$$m_{\mathrm{AB}} = -2.5 \log \frac{\int_{\lambda_i}^{\lambda_f} \lambda f_\lambda T_\zeta \, \mathrm{d}\lambda}{f_\nu^0 c \int_{\lambda_i}^{\lambda_f} \frac{T_\zeta}{\lambda} \mathrm{d}\lambda}$$

$$= -2.5 \log \frac{\int_{\lambda_i}^{\lambda_f} \lambda f_\lambda T_\zeta \, \mathrm{d}\lambda}{f_\lambda^0 \int_{\lambda_i}^{\lambda_f} \lambda T_\zeta \, \mathrm{d}\lambda} - 2.5 \log \frac{f_\lambda^0}{f_\nu^0 c}$$

$$- 2.5 \log \frac{\int_{\lambda_i}^{\lambda_f} \lambda T_\zeta \, \mathrm{d}\lambda}{\int_{\lambda_i}^{\lambda_f} \frac{T_\zeta}{\lambda} \mathrm{d}\lambda}, \tag{6}$$

where the dimensionless quantity $-2.5 \log \frac{f_\lambda^0}{f_\nu^0 c} = 18.6921$. With $\lambda_{\mathrm{PIVOT},\zeta} = \left(\frac{\int \lambda T_\zeta \mathrm{d}\lambda}{\int \frac{T_\zeta}{\lambda} \mathrm{d}\lambda} \right)^{1/2}$, we obtain

$$m_{\mathrm{AB}} = m_{\mathrm{ST}} - 5 \log \lambda_{\mathrm{PIVOT},\zeta} + 18.6921. \tag{7}$$

From equation (7), it follows that AB and ST magnitudes are identical at a wavelength $\simeq 5475$ Å. As Oke & Gunn (1983) chose to use the absolute flux of α Lyr (Vega) at 5480 Å to define the wavelength[3] at which $m_{\mathrm{AB}} = m_{\mathrm{VEGA}}$, the flux values f_ν^0 and f_λ^0 are chosen so that, for convenience, α Lyr has very similar magnitudes in all systems, ST, AB, and VEGA. Note that a revision of the actual flux scale of α Lyr (or any network of spectrophotometric standards) affects only the way that photometric observations are standardized to those systems, not their definitions. (That is, when standardizing observations, zero-point shifts can be applied in order to exactly match the original definitions).

2.5 VEGA mag system

This system, which is the most well-known one, uses α Lyr (Vega) as the primary calibrating star, as in the case of the most famous and still widely used Johnson–Cousins system (and many others). Historically, the zero-points of the Johnson system were defined 'in terms of unreddened main-sequence (MS) stars of class A0 . . . with an accuracy sufficient to permit the placement of the zero-point to about 0.01 mag' (Johnson & Morgan 1953). While observationally this zero-point is often defined by a network of standard stars, formally it can be anchored to just one object, the usual choice being α Lyr. The definition of the VEGA system is given only for heterochromatic measurements

$$m_{\mathrm{VEGA}} = -2.5 \log \frac{\int_{\lambda_i}^{\lambda_f} \lambda f_\lambda T_\zeta \, \mathrm{d}\lambda}{\int_{\lambda_i}^{\lambda_f} \lambda T_\zeta \, \mathrm{d}\lambda} + ZP_\zeta, \tag{8}$$

where ZP_ζ is derived for each bandpass ζ using a star of known absolute flux $f_\lambda = f_\star$ and observed magnitude $m_{\mathrm{VEGA}} = m_{\star,\zeta}$ (e.g. where our adopted magnitudes for Vega are reported in the third column of Table 1; Bessell et al. 1998; Girardi et al. 2002; Casagrande, Portinari & Flynn 2006). Thus,

$$ZP_\zeta = m_{\star,\zeta} + 2.5 \log \frac{\int_{\lambda_i}^{\lambda_f} \lambda f_\star T_\zeta \, \mathrm{d}\lambda}{\int_{\lambda_i}^{\lambda_f} \lambda T_\zeta \, \mathrm{d}\lambda} = m_{\star,\zeta} + 2.5 \log \bar{f}_{\star,\zeta}, \tag{9}$$

where $\bar{f}_{\star,\zeta}$ is the absolute calibration of the photometric system in the ζ band. ZP_ζ is thus of crucial importance for the synthetic photometry that we want to generate. To achieve the correct standardization, it is possible to modify either the adopted absolute calibration or the standard magnitude observed in the ζ band (or both). When generating synthetic magnitudes, an evaluation of both quantities must be provided (see Table 1).

As already noted, α Lyr is commonly used as the zero-point standard. Should its theoretical spectrum F_λ (see next section) be modelled with sufficient precision, and its angular diameter θ accurately measured, its absolute flux would be straightforward to obtain. In practice, its pole-on and rapidly rotating nature, as well as its suspected variability (although longward of 12 μm; Aumann et al. 1984, and thus of no impact on the colours investigated here) complicate things (also see the discussion in Casagrande et al. 2006). In practice, the best approach resorts to the use of a composite absolutely calibrated spectrum for different wavelength regions. Arguably, the best absolute flux $f_\star$ for α Lyr is currently available from the CAL-SPEC library,[4] which intermingles *Hubble Space Telescope* (*HST*) absolute spectrophotometry in the range 1675–5350 Å, with an especially tailored model flux longward of this wavelength. The overall accuracy of this absolute flux is ~ 1 per cent (Bohlin 2007), which translates to about 0.01 mag in ZP_ζ. If not otherwise specified, this is the absolute flux that we have used when generating synthetic magnitudes in the VEGA system.

2.6 Reality check

It follows from the previous sections that the formalism to define a photometric system is sound, independently of whether the ST, AB, or VEGA system is used. However, its actual realization at the telescope is far from being simple (see also Bessell 2005). Factoring in all possible sources of uncertainty in terms of the quantities we are discussing here means that the absolute flux, as well as the magnitudes, of the standard star might not be accurate (nor precise) enough (as is probably the case for α Lyr), and/or the actual system transmission curves might not be in exact agreement with those tabulated. In fact, more often than not, (small) zero-point corrections are still needed to replicate the definition of a given photometric system as closely as possible (and more generally, linear terms rather than zero-points might even be more appropriate, even though they are rarely, if ever, considered). That is, for certain filters, a correction term ϵ_ζ might be added to the right-hand sides of equations (3), (5), and (8). Table 1 reports when such corrections are necessary. It is worth mentioning that these corrections depend on the definitions adopted for each photometric system; consequently, different authors might use opposite signs. The values listed here comply with the definitions adopted in this paper.

2.7 Bolometric corrections

Libraries of synthetic stellar spectra provide the flux on a surface element F_λ (usually in erg s^{-1} cm^{-2} Å^{-1}) for a given set of stellar parameters (see Section 3) from which it is straightforward to compute the theoretical absolute flux

$$f_\lambda = 10^{-0.4 A_\lambda} \left(\frac{R}{d} \right)^2 F_\lambda, \tag{10}$$

---

[3] Note that Oke & Gunn (1983) adopted $V = 0.03$ for α Lyr, from which $m_{\mathrm{AB}} \sim V$ once the absolute flux at 5556 Å measured by Hayes & Latham (1975) 3.50×10^{-20} erg s^{-1} cm^{-2} Hz^{-1} was adopted. For an object with a relatively flat spectrum, this implied that $m_{\mathrm{AB}} = 0$ at f_ν^0, i.e. close to the value of 3.65×10^{-20} erg s^{-1} cm^{-2} Hz^{-1} measured by Oke & Schild (1970) at 5480 Å for a star of $V = 0.0$.

[4] Regularly updated absolute spectrophotometry can be found at http://www.stsci.edu/hst/observatory/cdbs/calspec.html. If not otherwise specified, we have used the STIS005 spectrum in this investigation.

for a star of radius R, at a distance d, and (if present) suffering from interstellar extinction of magnitude A_λ at wavelength λ. Such theoretical determinations of f_λ can then be inserted into the formalism outlined in the previous sections in order to compute synthetic magnitudes. Often only synthetic colours (i.e. the difference in the magnitudes measured through two filters) are computed, since doing so cancels out the dependence on the dilution factor $\frac{R}{d} = \frac{\theta}{2}$. Similarly, if one wishes to compute the BC in a given band BC_ζ

$$BC_\zeta = m_{\mathrm{Bol}} - m_\zeta = M_{\mathrm{Bol}} - M_\zeta, \tag{11}$$

where the lower and upper cases refer to apparent and absolute magnitudes, respectively. For simplicity, when dealing with synthetic fluxes, we use the same dilution factor $R_\odot/d_{10}$ for all models, where $d_{10} = 10\,\mathrm{pc}$, i.e. for the solar spectrum, we also compute its absolute magnitudes. For any models, it follows that

$$M_\zeta = -2.5 \log\left[\left(\frac{R_\odot}{d_{10}}\right)^2 \mathcal{K}_\zeta\right] + zp_\zeta, \tag{12}$$

where the exact form of zp_ζ (which now includes ϵ_ζ, if necessary) and $\mathcal{K}_\zeta$ (i.e. the integration of f_λ over the system response function) depends whether synthetic magnitudes are computed according to equations (3), (5), or (8). Also, from the definition of the absolute bolometric magnitude

$$M_{\mathrm{Bol}} = -2.5 \log \frac{R^2 T_{\mathrm{eff}}^4}{R_\odot^2 T_{\mathrm{eff},\odot}^2} + M_{\mathrm{Bol},\odot}, \tag{13}$$

because of the above choice on the dilution factor, the BC then becomes

$$BC_\zeta = -2.5 \log\left(\frac{T_{\mathrm{eff}}}{T_{\mathrm{eff},\odot}}\right)^4 + M_{\mathrm{Bol},\odot}$$
$$+ 2.5 \log\left[\left(\frac{R_\odot}{d_{10}}\right)^2 \mathcal{K}\right] - zp_\zeta. \tag{14}$$

In this paper, we have adopted $M_{\mathrm{Bol},\odot} = 4.75$, but it should be appreciated that this value is simply a *definition*, not a measurement. In fact, BCs were originally defined in the visual only, in such a way as to be negative for all stars (Kuiper 1938). From the spectral energy distribution, we expect BCs in the visual to be largest for very hot and for very cool stars. The minimum would then occur around spectral type F, which then would set the zero-point of the bolometric magnitudes. For the Sun, this implied a value $BC_{V,\odot}$ between -0.11 (Aller 1963) and -0.07 (Morton & Adams 1968). However, with the publication of a larger grid of model atmospheres, e.g. the smallest BC in the Kurucz's grid (1979) implied $BC_{V,\odot} = -0.194$. These difficulties can instead be avoided by adopting a fixed zero-point, which is currently the preferred choice. Therefore, any value of $M_{\mathrm{Bol},\odot}$ is equally legitimate, on the condition that once chosen, all BCs are rescaled accordingly (e.g. Torres 2010). As a matter of fact, whenever bolometric magnitudes are published, be they apparent or absolute, the adopted $M_{\mathrm{Bol},\odot}$ should always be specified.[5] We also note that using the solar values reported in Table 2, our choice implies $-0.07 \lesssim BC_{V,\odot} \lesssim -0.06$.

[5] It follows from equation (13) that adopting $M_{\mathrm{Bol},\odot} = 4.75$ with the GONG collaboration solar luminosity value $3.846 \times 10^{26}\,\mathrm{W}$, a star with $M_{\mathrm{Bol}} = 0$ has a radiative luminosity of $3.055 \times 10^{28}\,\mathrm{W}$, which is the flux zero-point of the BC scale according to the definitions adopted by IAU Commissions 25 and 36 at the IAU 1997 General Assembly.

Table 2. Solar absolute magnitudes, obtained using the MARCS synthetic solar spectrum ($\xi = 1\,\mathrm{km\,s^{-1}}$, $T_{\mathrm{eff}} = 5777\,\mathrm{K}$, $\log g = 4.44$ and [Fe/H] = 0.0) and by interpolating in the $\xi = 2\,\mathrm{km\,s^{-1}}$ grid on the assumption of the same physical parameters. The filters are the same as in Table 1.

M_ζ	Solar	grid
UX	5.569	5.615
BX	5.427	5.438
B	5.444	5.455
V	4.823	4.818
R_C	4.469	4.459
I_C	4.129	4.120
U	5.584	5.631
B	5.435	5.446
V	4.814	4.808
R_C	4.453	4.444
I_C	4.126	4.118
J	3.650	3.643
H	3.362	3.359
K_S	3.277	3.274
u	6.430	6.479
g	5.075	5.079
r	4.649	4.640
i	4.535	4.526
z	4.508	4.500
$F435W_{\mathrm{ACS}}$	5.442	5.454
$F475W_{\mathrm{ACS}}$	5.169	5.172
$F555W_{\mathrm{ACS}}$	4.832	4.827
$F606W_{\mathrm{ACS}}$	4.631	4.623
$F814W_{\mathrm{ACS}}$	4.109	4.100
$F218W$	9.220	9.263
$F225W$	8.446	8.517
$F275W$	6.986	7.063
$F336W$	5.465	5.523
$F350LP$	4.751	4.748
$F390M$	5.987	6.018
$F390W$	5.611	5.638
$F438W$	5.447	5.460
$F475W$	5.146	5.149
$F547M$	4.800	4.794
$F555W$	4.868	4.864
$F606W$	4.639	4.632
$F625W$	4.493	4.484
$F775W$	4.156	4.147
$F814W$	4.115	4.106
$F850LP$	4.001	3.993
$F098M$	3.956	3.949
$F110W$	3.787	3.780
$F125W$	3.662	3.656
$F140W$	3.520	3.515
$F160W$	3.393	3.390

Notes: HST magnitudes are all in the VEGA system.

2.8 Caveats with extinction

Before dealing with extinction, it is useful to clarify the wavelength with which heterochromatic measurements (magnitudes in this case) are associated. Any heterochromatic measurement can always be reduced to a monochromatic flux $\bar{f}$ (also called effective flux) via

$$\bar{f} = \frac{\int_{\lambda_i}^{\lambda_f} \lambda f_\lambda T_\zeta \, \mathrm{d}\lambda}{\int_{\lambda_i}^{\lambda_f} \lambda T_\zeta \, \mathrm{d}\lambda}. \tag{15}$$

Assuming that the function f_λ is continuous and that T_ζ does not change sign in the interval (λ_i, λ_f), the generalization of the mean value theorem states that there is at least one value of λ in the above interval such that

$$f_{\tilde{\lambda}} \int_{\lambda_i}^{\lambda_f} \lambda T_\zeta \, \mathrm{d}\lambda = \int_{\lambda_i}^{\lambda_f} \lambda f_\lambda T_\zeta \, \mathrm{d}\lambda. \tag{16}$$

Rearranging this, we obtain

$$\bar{f} = f_{\tilde{\lambda}} = \frac{\int_{\lambda_i}^{\lambda_f} \lambda f_\lambda T_\zeta \, \mathrm{d}\lambda}{\int_{\lambda_i}^{\lambda_f} \lambda T_\zeta \, \mathrm{d}\lambda}, \tag{17}$$

where $\tilde{\lambda}$ is the isophotal wavelength. The latter is thus the wavelength which must be attached to the monochromatic quantity $\bar{f}$ that is obtained from a heterochromatic measurement. Stellar spectra do not necessarily satisfy the requirement of the mean value theorem for integration, as they exhibit discontinuities. Although the mean value of the intrinsic flux is well defined, the determination of the isophotal wavelength becomes problematic because spectra contain absorption lines, and hence the definition of $\tilde{\lambda}$ can yield multiple solutions (e.g. Tokunaga & Vacca 2005; Rieke et al. 2008). It is possible to avoid these complications by introducing the effective wavelength (here in photon-counting formalism)

$$\lambda_{\mathrm{eff}} = \frac{\int_{\lambda_i}^{\lambda_f} \lambda^2 f_\lambda T_\zeta \, \mathrm{d}\lambda}{\int_{\lambda_i}^{\lambda_f} \lambda f_\lambda T_\zeta \, \mathrm{d}\lambda}, \tag{18}$$

i.e. the mean wavelength of the passband weighted by the energy distribution of the source over that band, which is a good approximation for $\tilde{\lambda}$ (Golay 1974). The effective wavelength thus shifts with f_λ, depending on the source under investigation since it depends on both the extinction and the intrinsic stellar spectrum (equation 10). If present, extinction is usually parametrized as follows: $A_\lambda = R_V E(B - V)[a(\lambda^{-1}) + b(\lambda^{-1})/R_V]$, where $E(B - V)$ is the colour excess (or reddening) and $R_V \equiv \frac{A_V}{E(B-V)}$ is the ratio of total to selective extinction in the optical, assumed to be constant $\simeq 3.1$ for most line of sights (e.g. Cardelli, Clayton & Mathis 1989). The above parametrization is known as the extinction law. Note that the extinction law is derived primarily using early O- and B-type stars, i.e. it is expressed in terms of an $A_V = R_V E(B - V)$ relation that is valid for these spectral types. Also, despite being given in a monochromatic form (i.e. with a λ dependence), it is actually derived using photometric (i.e. heterochromatic) quantities, which are valid at the effective wavelengths appropriate for the stars plus filters used to derive the extinction law. While the implication of these facts is discussed in the literature (e.g. Fitzpatrick 1999; McCall 2004; Maíz Apellániz 2013), their importance is often overlooked. We call the R_V and $E(B - V)$ values which enter the extinction law 'nominal'. The amount of attenuation in a given bandpass ζ (i.e. the magnitude difference, where the subscript 0 indicates an unreddened source) is then

$$m_\zeta - m_{\zeta,0} = -2.5 \log \frac{\int_{\lambda_i}^{\lambda_f} \lambda 10^{-0.4 A_\lambda} F_\lambda T_\zeta \, \mathrm{d}\lambda}{\int_{\lambda_i}^{\lambda_f} \lambda F_\lambda T_\zeta \, \mathrm{d}\lambda} = A_\zeta, \tag{19}$$

and a given nominal $E(B - V)$ and R_V will produce a different effective flux associated with a different effective wavelength, depending on the intrinsic spectral energy distribution F_λ of the source under investigation. In other words, the colour excess between two bands $E(\zeta - \eta) = A_\zeta - A_\eta$ will vary with spectral class as well as with $E(B - V)$ and R_V. For example, assuming $R_V = 3.1$, the ratio $E(u - z)/E(B - V)$ in a metal-poor subgiant star ([Fe/H] $= -3.0$, $\log g = 3.5$, $T_{\mathrm{eff}} = 6500$ K) will vary from 3.333 to 3.319 assuming

a nominal $E(B - V) = 0.01$ or 0.70, respectively. The same ratio will be 3.283 or 3.275 in a solar metallicity giant ($\log g = 2.0$, $T_{\mathrm{eff}} = 4000$ K), and 3.375 or 3.362 in a solar metallicity M dwarf ($\log g = 5.0$, $T_{\mathrm{eff}} = 2500$ K). If $R_V = 2.5$, which seems to be representative of selected directions towards the bulge (Nataf et al. 2013), the aforementioned numbers would change to 3.188 and 3.164 (metal-poor subgiant), 3.123 and 3.108 (solar metallicity giant), and 3.211 and 3.187 (solar metallicity M dwarf).

Based on the above considerations, it is also important to stress that the nominal R_V and $E(B - V)$ values entering the extinction law – as derived from early-type stars – change when moving towards later spectral types as a result of the change in effective wavelength. As an example, in the case of a late-type star, the effective wavelengths of the B and V filters shift to longer wavelengths, where the extinction decreases, lowering both A_B and A_V for a given amount of dust. As a result, $R_V = \frac{A_V}{E(B-V)} = \frac{A_V}{A_B - A_V}$ increases (even if the amount and physical properties of the dust are the same!) because the decrease in the denominator of this ratio overwhelms the decrease of the numerator. Thus, it is important to take this effect into account to distinguish whether a variation in R_V stems from shifts in the effective wavelengths or from changes in the nature of the dust (see e.g. the excellent discussion in McCall 2004). For reference, a nominal $R_V = 3.1$ and $E(B - V) = 0.60$ in the aforementioned extinction law return $R_V = 3.4$ and $E(B - V) = 0.55$ for a moderately metal-poor turn-off (TO) star. (We will elaborate on our discussion of this practical example in Section 5 and Appendix A.)

These subtleties are usually neglected when, e.g. isochrones are fitted to the CMDs of halo globular clusters that have low values of the reddening, but they might not be negligible if the object under consideration is in a heavily obscured region of the Galactic disc or bulge. Furthermore, when using an $E(B - V)$ value from the literature, it should be kept in mind how this value was obtained; i.e. whether it is based on stars (and if so, which spectral types; e.g. Schlafly & Finkbeiner 2011), or even background galaxies (e.g. Schlegel, Finkbeiner & Davis 1998). Indeed, because of the above issues, it should not come as a surprise to find that small adjustments to literature values of $E(B - V)$ are needed to obtain a satisfactory fit an isochrone to a given CMD (though this is just one of many possible causes of discrepancies between predicted and observed colours). In addition, as we already pointed out, the use of a constant colour excess across the entire CMD is not optimal in the presence of high extinction. We discuss in Section 5 how the set of reddened colours provided in this investigation enables one to address these subtleties.

2.9 Johnson–Cousins $UBV(RI)_C$ and 2MASS JHK_S

Synthetic colours in the Johnson–Cousins and 2MASS filter sets have been computed in the VEGA system only, and they have already been used in the investigations by VandenBerg et al. (2010) and Brasseur et al. (2010), where further details can be found. Briefly, the absolute calibration of the Johnson–Cousins system is obtained using the updated CALSPEC absolute spectrophotometry[6]

---

[6] At the time of generating those magnitudes, the most updated spectrum available was the STIS003, which underpins the absolute calibration of the Johnson–Cousins system reported in Table 1. Should e.g. the STIS005 spectrum be used, the Johnson–Cousins absolute fluxes in Table 1 would change into $UX = 4.0027$E-9, $BX = 6.2313$E-9, $B = 6.2763$E-9, and $V = 3.6112$E-9 erg s^{-1} cm^{-2} Å^{-1}, thus implying magnitude differences of 0.007 in UX, BX, and B and 0.002 in V band. The fluxes in R_C and I_C would remain identical.
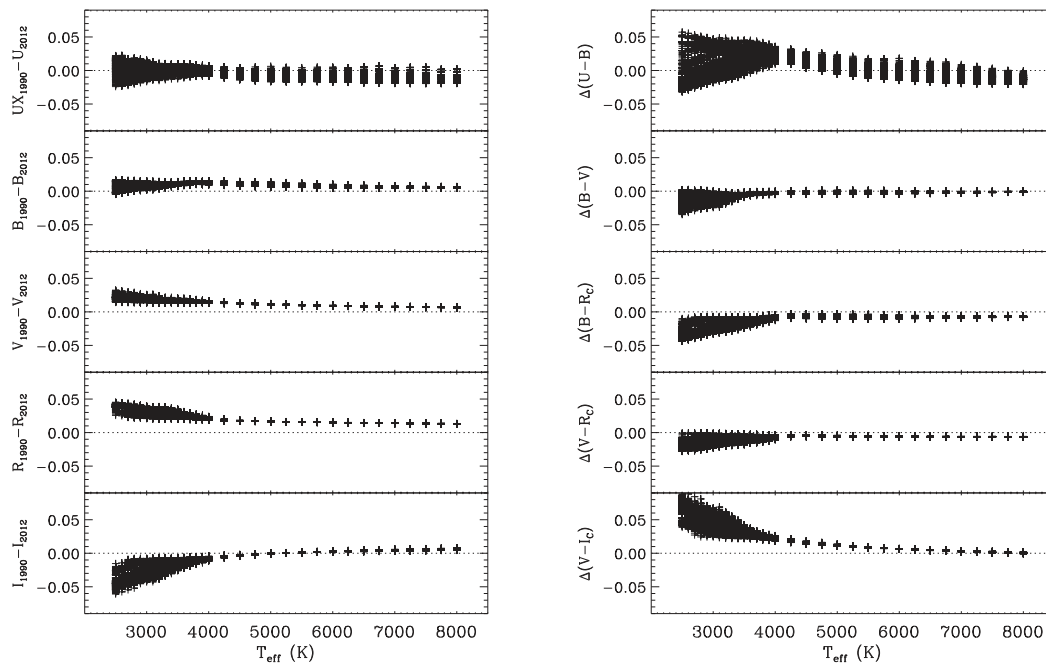
Figure 2. Left panels: difference between the `ubvri90` and `ubvri12` magnitudes. Each point is a model flux of different T_{eff}, log g and [Fe/H], according to the values available from the MARCS library (α-standard composition). Right panels: same difference for selected colour indices.

of α Lyr (Bohlin 2007) and the filter transmission curves of Bessell (1990b): the results are forced to match the observed magnitudes of Vega (Bessell 1990a). Because of problems standardizing the U magnitudes, Bessell (1990b) provides two transmission curves for the B system: one dubbed 'BX' to be used in conjunction with 'UX' for the computation of the $U - B$ colour index, and the other labelled 'B' for use with any of the redder bandpasses $V(RI)_C$ to calculate, e.g. $B - V$ or $V - I_C$ colours. We have chosen to use the name `ubvri90` to identify these magnitudes.

An additional set of synthetic Johnson–Cousins colours has also been computed following the prescriptions of Bessell & Murphy (2012), i.e. using improved filter transmission curves for the U and B bands (thereby removing the need to distinguish between, e.g. 'BX' and 'B') and newly derived zero-points. The novel approach of Bessell & Murphy (2012) is that the Johnson–Cousins system is formulated in terms of AB magnitudes, despite being on the VEGA system. We have named these magnitudes `ubvri12`. It is very comforting to find that the differences between the two sets of Johnson–Cousins magnitudes are relatively minor and essentially constant, never exceeding 0.02 mag (0.05 mag) above (below) 4000 K. The same is also true when colour indices are compared instead of magnitudes; with regard to BVR_C, in particular, the constant offsets found in magnitudes conspire to give nearly the same colours above 4000 K (see Fig. 2).

For the 2MASS JHK_S system, the α Lyr magnitudes, absolute calibration, and system response functions of Cohen, Wheaton & Megeath (2003) are used, including the small zero-point corrections found in Casagrande et al. (2010). The difference with respect to the CALSPEC absolute flux in the near-IR is minor (see discussion in Casagrande et al. 2010), and our choice is motivated by the fact that the 2MASS absolute calibration adopted here has been thoroughly tested (Rieke et al. 2008; Casagrande et al. 2012). Note that both Bessell (1990b) and Cohen et al. (2003) system response functions are photon-counting, i.e. they are already multiplied by λ and renormalized. Thus, T_ζ (not λT_ζ) must be used in the equations

of synthetic photometry (Section 2). With these choices, the absolute calibration in these filters is essentially identical to that underlying the T_{eff} scale of Casagrande et al. (2010) and verified via analyses of solar twins.[7]

2.10 Sloan Digital Sky Survey *ugriz*

Sloan Digital Sky Survey (SDSS) photometry is defined to be on the AB system, although small post-facto zero-point corrections are necessary (Eisenstein et al. 2006; Holberg & Bergeron 2006). We have generated AB magnitudes using the SDSS filter transmission curves[8] and determined the necessary zero-point corrections ϵ_ζ using stars with absolute flux measurements from the CALSPEC library and having SDSS *ugriz* measurements (Casagrande et al., in preparation).

Two remarks must be made: first, the exact definition of SDSS magnitudes is on the asinh system, where the classical Pogson logarithmic scale (Section 2.1) is replaced by the inverse hyperbolic sine function ('asinh magnitudes'; see Lupton, Gunn & Szalay 1999). Conveniently, this definition is virtually identical to the standard Pogson magnitudes at high signal to noise, but it behaves better at magnitudes fainter than the detection repeatability limit (i.e. much fainter than 20th mag for SDSS). Brighter than this threshold, the difference between the asinh and Pogson magnitudes is negligible and rapidly goes to zero. This makes the Pogson formulation outlined so far fully appropriate for generating synthetic magnitudes,

---

[7] The only difference is the $BV(RI)_C$ absolute calibration in Casagrande et al. (2010), which is based on earlier *HST* spectrophotometry of α Lyr (as reported in table A2 of Casagrande et al. 2006), producing T_{eff} values that differ by only a few Kelvin. However, this difference essentially cancels out when the solar twins are used in the calibrating process; i.e. the absolute calibration derived from Bohlin (2007) agrees with that based on the solar twins.

[8] http://www.sdss3.org/instruments/camera.php#Filters

besides being more convenient given the dependence of the asinh magnitudes[9] on a softening parameter (survey dependent) and the difficulty of defining quantities such as BCs and absolute magnitudes in the asinh formulation (see e.g. Girardi et al. 2004).

The second remark concerns the potential confusion between the *primed u'g'r'i'z'* and *unprimed ugriz* magnitudes. The basis of the photometric calibration of the SDSS is defined by the 158 primary standards measured by the USNO 40-inches telescope (Smith et al. 2002), which however has filters with different effective wavelengths than those of the SDSS 2.5 m survey telescope.[10] The latter defines the *unprimed ugriz* system for which photometry has been published from SDSS DR1 onwards, and for which we provide synthetic colours in this work. *Primed* magnitudes should thus be transformed into the *unprimed* system before comparing and/or using them with the synthetic photometry published here (see e.g. Tucker et al. 2006).

2.11 *HST*

The distinctive feature of *HST* photometry is the use of the `AB` and `ST` systems, in addition to the `VEGA` system. We have generated BCs and colours for a number of filters commonly used in two instruments: the Advanced Camera for Surveys (ACS) is a third generation *HST* instrument which has provided some of the deepest photometric optical images ever obtained (Sarajedini et al. 2007), while the Wide Field Camera 3 (WFC3) is a fourth generation instrument (replacing the Wide Field Planetary Camera 2, WFPC2) that covers the electromagnetic spectrum from UV to the IR. For both cameras, a large number of filters is available, covering longpass (*LP*), broad (*W*), intermediate (*M*), and narrow (*N*) bands. Some of them closely match such commonly used filters as those in the Johnson–Cousins, SDSS, Strömgren, and Washington systems (e.g. Bessell 2005). To provide continuity with previous observations, several of the WFC3 filters are very similar to those used in the WFPC2 and ACS instruments (e.g. Rajan et al. 2011). We have produced transformations in the `AB`, `ST` and `VEGA` systems for the following filters: *F435W*, *F475W*, *F555W*, *F606W*, and *F814W* (ACS camera); *F218W*, *F225W*, *F275W*, *F336W*, *F350LP*, *F390M*, *F390W*, *F438W*, *F475W*, *F547M*, *F555W*, *F606W*, *F625W*, *F775W*, *F814W*, *F850LP* (WFC3 optical) and *F098M*, *F110W*, *F125W*, *F140W*, *F160W* (WFC3 infrared).

Updated values for the system response functions as well as regular improvements to the absolute flux of α Lyr are provided by the *HST* team. We list in Table 1 our adopted values. The absolute calibration of α Lyr that we derived for the ACS system differs slightly from the values currently listed in the website.[11] These differences in absolute flux correspond to zero-point shifts of ≃0.01 mag in *F435W* and <0.005 mag in the other ACS filters considered here. At any given time, users can readily compute the difference in magnitude implied by the $\bar{f}_\star$ that we adopted, and they may use any updated/preferred value, shifting if necessary our computed colours by this amount.

We conclude this section with a cautionary note: particular care should be taken when working with stars that have cool effective temperatures and/or high value of reddening (the exact values of these quantities depend on the filter being used). Some of the UV

filters are known to have red leaks towards longer wavelengths. Although these leaks are usually confined to much less than 1 per cent, they may not be negligible in some cases (see table 6.5 in Rajan et al. 2011), which could cause the synthetic colours to be anomalous and the effective wavelengths to be considerably redder than the values expected from the nominal filter bandpasses.

3 MARCS SYNTHETIC LIBRARY

Magnitudes and colours have been computed using the MARCS grid of synthetic stellar spectra,[12] which is available for $2500 \leq T_{\rm eff}({\rm K}) \leq 8000$ (in steps of 100 K below 4000 K, and 250 K above this limit), $-0.5 \leq \log g \leq 5.5$ (in steps of 0.5 dex) and different chemical compositions (Gustafsson et al. 2008). In all instances, a microturbulence $\xi = 2\,{\rm km\,s^{-1}}$ has been adopted: we discuss later the effect of changing this parameter.

The reference solar abundance mixture is that of Grevesse, Asplund & Sauval (2007). All radiative transfer is treated assuming local thermodynamic equilibrium. The bulk of the synthetic colours has been computed using MARCS model fluxes assuming the so-called standard chemical composition (α-standard); i.e. a metal mixture that reflects the values of [α/Fe] typically observed in solar neighbourhood stars. To be specific, [α/Fe] = 0.4 for [Fe/H] ⩽ −1.0, [α/Fe] = 0.0 for [Fe/H] ⩾ 0.0, and [α/Fe] decreasing linearly from 0.4 to 0.0 for −1.0 ⩽ [Fe/H] ⩽ 0.0. While this α-enrichment is broadly representative of field stars in the Galactic disc and halo (e.g. Edvardsson et al. 1993; Nissen et al. 1994; Fuhrmann 2008), different abundance ratios can be more appropriate for other stellar populations, where the trend of [α/Fe] versus metallicity depends primarily on the initial mass function and the star formation rate (e.g. Tinsley 1979; McWilliam 1997; Tolstoy, Hill & Tosi 2009). Models with different [α/Fe] are available from the MARCS website and we have generated additional synthetic colours for the following cases: (i) α-enhanced (i.e. [α/Fe] = 0.4 above [Fe/H] = −1.0), (ii) α-poor (i.e [α/Fe] = 0.0 below [Fe/H] = 0.0), and (iii) α-negative (i.e [α/Fe] = −0.4 from supersolar to metal-poor). The MARCS library covers the range −5.0 ⩽ [Fe/H] ⩽ 1.0, although for certain combinations of stellar parameters the grid contains relatively few models. As discussed in Appendix A, computer programs have been provided to generate BCs (and hence colour indices) for nearly the entire MARCS grid as it presently exists.

When computing synthetic magnitudes, we assume one solar radius at a 10 pc distance for all models, i.e. $f_\lambda = 10^{-0.4A_\lambda}(\frac{R_\odot}{d_{10}})^2 F_\lambda$. While this choice is arbitrary (and actually irrelevant), it has the practical advantage that BCs can be computed very easily from synthetic magnitudes (see equation 14). To determine the effect of varying the $E(B - V)$ from 0.0 to 0.72 on the BCs, we reddened each theoretical flux using the extinction law of O'Donnell (1994) in the range 3030–9090 Å and the one by Cardelli et al. (1989) everywhere else. In all instances, we adopted $R_V = 3.1$: an extension of our computations to other values of R_V is currently in progress.

3.1 The role of microturbulence

In one-dimensional model atmospheres, the microturbulence ξ is a free parameter which is introduced to broaden spectral lines when synthesizing a spectrum. It conserves the width of weak lines, and it can reduce the saturation of strong lines, thus increasing their total absorption. Its physical interpretation is that of a non-thermal

---

[9] https://www.sdss3.org/dr10/algorithms/magnitudes.php#asinh
[10] see http://www.sdss.org/dr7/algorithms/fluxcal.html for an extensive explanation
[11] http://www.stsci.edu/hst/acs/analysis/zeropoints/#vega
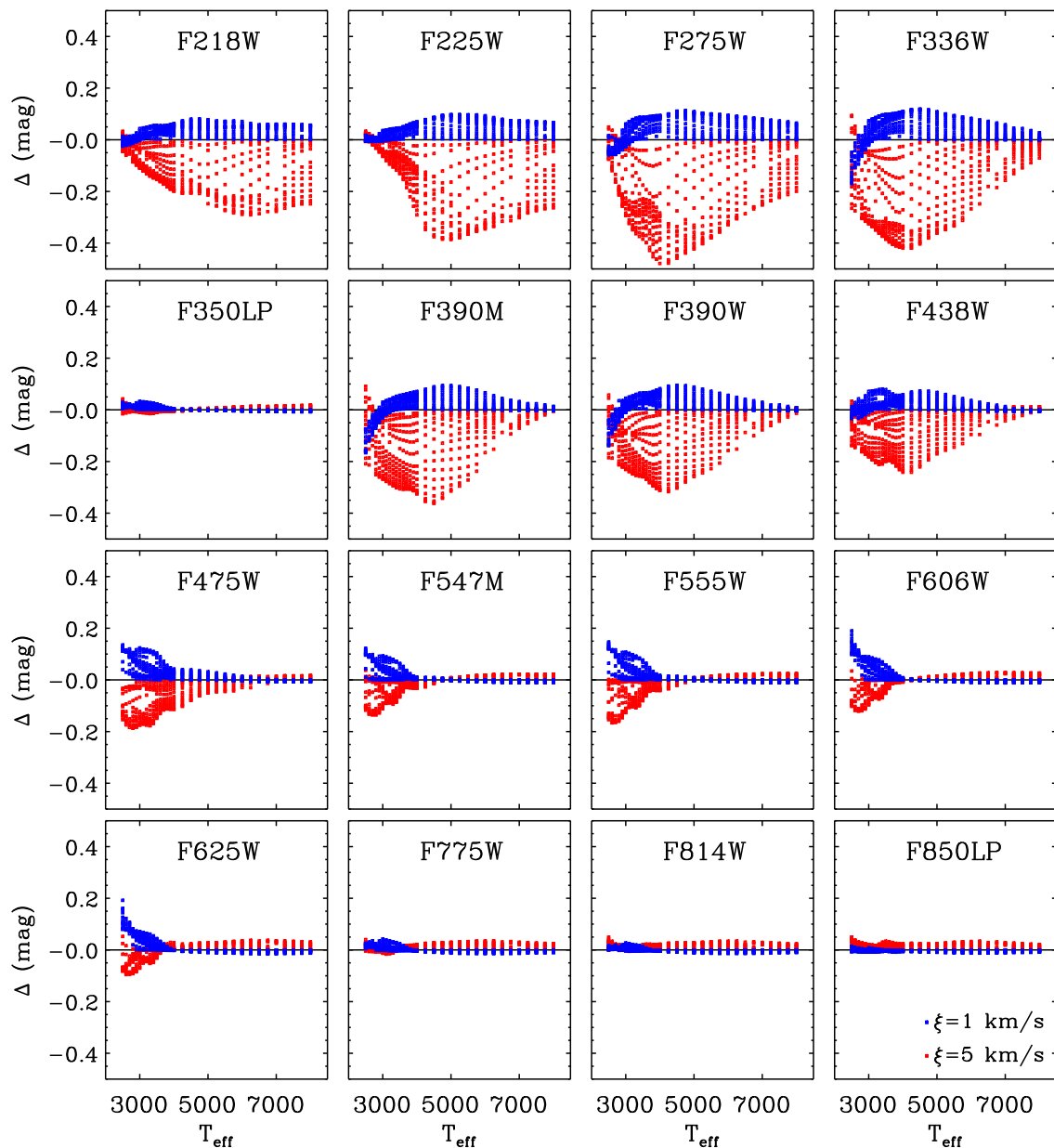
[12] http://marcs.astro.uu.se

Figure 3. Difference in synthetic magnitudes and BC_ζ as function of model T_{eff} when using a microturbulence of $1\,km\,s^{-1}$ (blue) or $5\,km\,s^{-1}$ (red) with respect to standard value of $\xi = 2\,km\,s^{-1}$. The filter used is indicated in each panel. In all instances, models with α-standard composition have been used. A fixed value of $\log g = 4.0$ and 2.5 has been used when comparing between 1 and $2\,km\,s^{-1}$ and 5 and $2\,km\,s^{-1}$, respectively.

small-scale motion (compared to unit optical depth, or the mean free path of a photon), stemming from the convective velocity field in a stellar atmosphere. Insofar as our investigation is concerned, the effect of microturbulence is to partly redistribute the flux in spectral regions that are crowded with lines, and thus its effects are expected to be more evident towards the blue and the UV, and in filters with smaller wavelength coverages.

There is no unique, nor clear-cut, relation between the microturbulence and stellar parameters, although the available evidence points towards ξ increasing at higher luminosities. For reference, a typical value for dwarfs and subgiants is around 1–$1.5\,km\,s^{-1}$, going up to 2–$2.5\,km\,s^{-1}$ for stars on the red-giant branch (RGB), and possibly as high as $5\,km\,s^{-1}$ in supergiants (e.g. Nissen 1981; Gray, Graham & Hoyt 2001; Allende Prieto et al. 2004; Roederer & Sneden 2011).

A constant value of $\xi = 2\,km\,s^{-1}$ is usually assumed in large grids of synthetic stellar spectra (e.g. Castelli & Kurucz 2004; Brott & Hauschildt 2005) and the same is true for the MARCS library as well. Fortunately, subsets of MARCS models that assume $\xi = 1$ and $5\,km\,s^{-1}$ are also available, which enables us to investigate how a change in the microturbulence affects synthetic magnitudes.[13]

Figs 3–4 compare the magnitudes which are obtained using $\xi = 1$ or $5\,km\,s^{-1}$ instead of $\xi = 2\,km\,s^{-1}$. Notice that it follows from equation (11) that these figures also illustrate the differences of

---

[13] It is for this reason that the colours which are obtained by interpolating in our transformation tables for the solar values of $\log g$, T_{eff} and metallicity are somewhat different from those derived from the MARCS synthetic spectrum for the Sun, which assumes $\xi = 1\,km\,s^{-1}$.
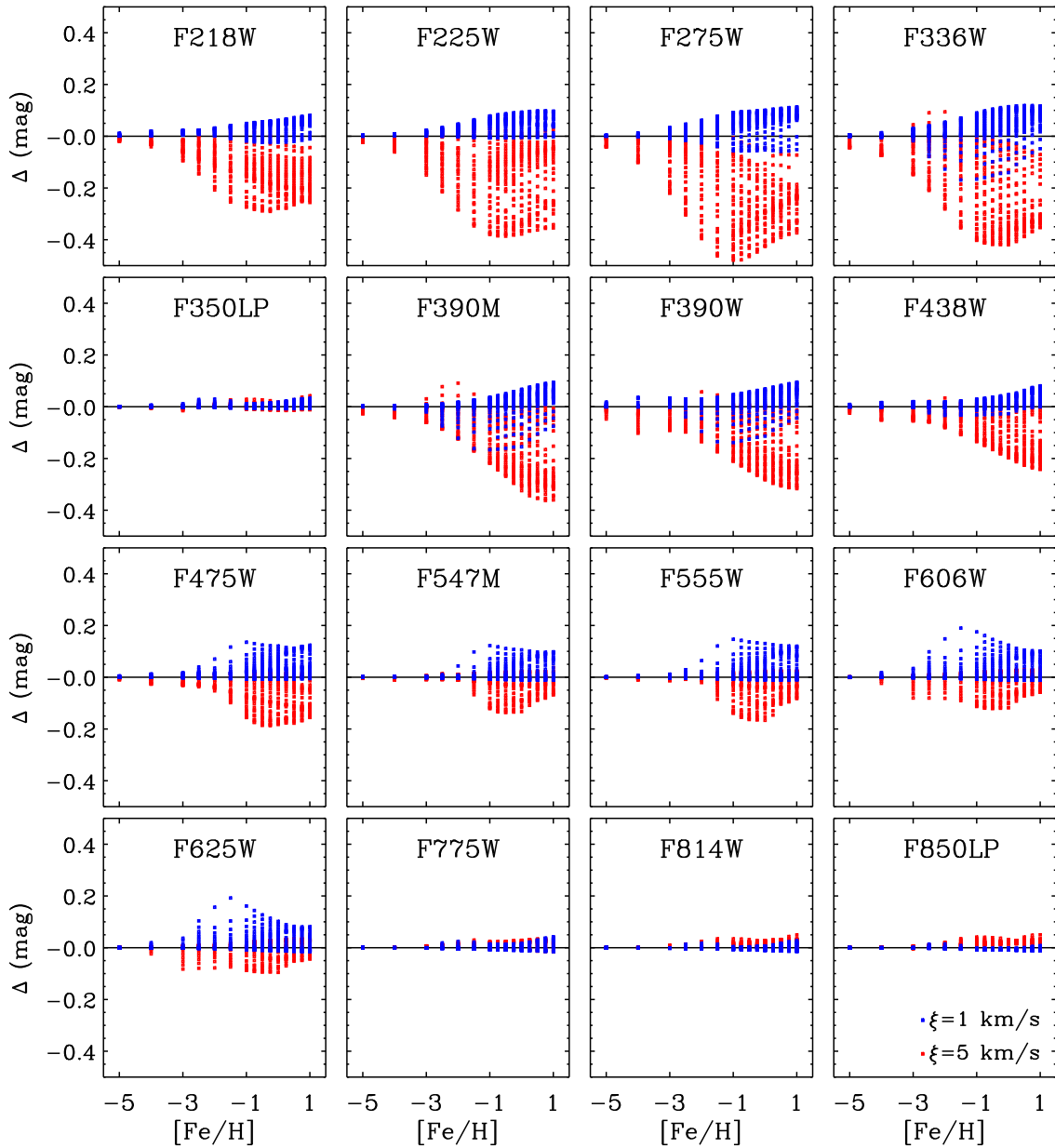
Figure 4. Same as Fig. 3, but as function of [Fe/H].

BC_ζ as a function of T_{eff} and [Fe/H]. We opted to use the WFC3 optical filters for this demonstration, as they are representative of most of the colours computed in this work, and they provide a rich diversity in terms of wavelength coverage and filter widths. For the blue and UV filters, the effects of microturbulence are significant at all T_{eff} values and they increase with increasing [Fe/H]: in certain cases, the differences are as much as 0.1 mag if ξ is reduced from 2 to 1 km s^{-1}, or up to 0.5 mag if the microturbulence is increased to $\xi = 5$ km s^{-1}. While such a high value of ξ might not be representative of the values commonly encountered in stars, it provides a very instructive example of how a fudge factor such as the microturbulence can impact synthetic colours. The only filter essentially unaffected by a change of ξ is $F350LP$, for which any flux redistribution occurs essentially within its very large bandpass ($\simeq$476nm). At wavelengths longer than about 5000 Å and for $T_{eff} \gtrsim 4000$ K, a change of ξ has less pronounced effects, typically of the order of,

or less than, a hundredth of a magnitude. Although not shown in the plots, we have verified that this is true also for near-IR colours (2MASS). In fact, these variations are at about the same level of the accuracy at which synthetic colours can be generated when taking into account zero-point and absolute calibration uncertainties.

The impact of microturbulence in cool stars must therefore be kept in mind when comparing models with observations at wavelengths roughly bluer than *V*, especially for objects which are known to have microturbulent velocities that depart considerably from the standard assumption of 2 km s^{-1}. This dependence on ξ clearly introduces an additional degree of freedom which can be avoided only by hydrodynamic simulations that treat the velocity field in a consistent manner (e.g. Steffen, Caffau & Ludwig 2013). At the present time, the impact of three-dimensional model atmospheres on synthetic colours is still largely unexplored (Kučinskas et al. 2005, 2009; Casagrande 2009), but hopefully the recent advent of

hydrodynamic grids of model atmosphere (Beeck et al. 2013; Magic et al. 2013; Tanner, Basu & Demarque 2013; Tremblay et al. 2013) will soon make such studies possible.

4 COMPARISONS WITH OBSERVATIONS

The testing of synthetic fluxes is normally done by comparing the observed and modelled spectral energy distributions for a range of wavelengths and spectral types (e.g. Edvardsson 2008; Bohlin 2010; Bessell 2011) or by comparing synthetic and observed colours in different bands and for different values of $T_{\rm eff}$, log g and [Fe/H] (e.g. Bessell et al. 1998; Önehag et al. 2009). Here, we follow the latter approach. First, we compare synthetic colours in different filters with observations of field stars that have well-determined physical parameters and magnitudes, as well as with empirical relations that link colours to stellar parameters. Then, we turn our attention to star clusters, which enable us to test the consistency of the fits of isochrones to the observed photometry on several different colour–magnitude planes.

Readers should bear in mind the caveats of generating synthetic photometry that have been discussed in Section 2, as well as the difficulty of standardizing photometric observations (ground based, in particular) to better than about 0.01 mag (e.g. Stetson 2005). Therefore, when comparing synthetic and observed colours, agreement to within 0.01–0.02 mag should usually be regarded as excellent.

4.1 The Sun and other field stars

Arguably, the Sun is the star with the best-known parameters, and it is the most important benchmark in stellar astrophysics. However, for obvious reasons, it cannot be observed with the same instruments and under the same conditions as more distant stars, thus making it virtually impossible to tie its colours to other photometric observations (e.g. Stebbins & Kron 1957). Recently, the use of solar analogues and twins has overcome this limitation, and reliable colours are now available in the Johnson–Cousins and 2MASS system (Casagrande et al. 2012; Ramírez et al. 2012). Fig. 5 compares these measurements with the colour indices obtained using the MARCS solar synthetic flux (open circles). Differences are usually well within 0.02 mag, which is approximately the conjugated uncertainty of the observed and synthetic colours, and hence the accuracy
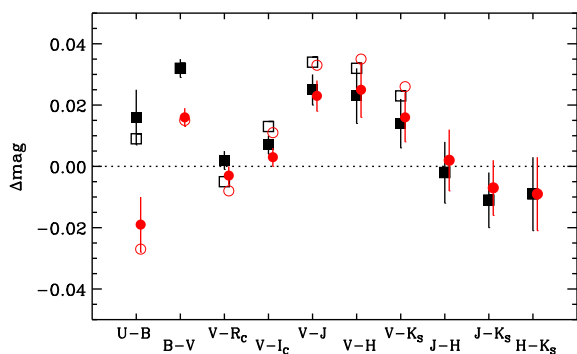

Figure 5. Solar synthetic colours compared to empirical determinations from Ramírez et al. (2012) and Casagrande et al. (2012). Squares are obtained using the MARCS solar flux (which has $\xi = 1\,{\rm km\,s^{-1}}$), while circles (slightly shifted on the abscissa for clarity) are from interpolations in the $\xi = 2\,{\rm km\,s^{-1}}$ MARCS grid at the solar values of $T_{\rm eff}$, log g, and [Fe/H]. Only the error bars from the above empirical determinations have been attached to the synthetic magnitudes. For the optical filters, filled and open symbols refer to the `ubvri90` and `ubvri12` transformations, respectively.

at which our colours are testable. Also shown in Fig. 5 is a similar comparison, but of colours which are obtained by interpolating in the $\xi = 2\,{\rm km\,s^{-1}}$ grid at the solar $T_{\rm eff}$, log g, and [Fe/H]. The differences with respect to those based on the solar synthetic spectrum are negligible longward of the V band, whereas at wavelengths bluer than the B band, they are more substantial (in accordance with the effects of microturbulance discussed in Section 3.1).

Fig. 6 shows the comparison between the observed and synthetic *ugriz* colours for a sample of about 13 500 stars in the SEGUE DR8 catalogue (Yanny et al. 2009), flagged to have good photometric quality in all bands, and to cover a broad range of stellar parameters as determined from the SSPP pipeline (Lee et al. 2011, and references therein). MARCS synthetic colours are clearly quite successful in reproducing the observed trends on the different colour planes as function of both [Fe/H] and log g, especially given that the SSPP values have their own measurement uncertainties. Also worth pointing out is the decreasing sensitivity of *ugriz* broad-band colours to [Fe/H] in the direction of reduced metallicities: note the reduced separations of the loci between $-1 \geqslant$ [Fe/H] $\geqslant -3$, and even more so between $-3 \geqslant$ [Fe/H] $\geqslant -5$.

For all of the stars in Fig. 6, we also determine $T_{\rm eff}$ and $f_{\rm Bol}$ using the Infrared Flux Method (IRFM) described in Casagrande et al. (2010). Briefly, multiband optical *ugriz* and IR JHK_S photometry is used to recover the bolometric flux of each star, from which its effective temperature can then be readily obtained. The method is to a large extent empirical: it depends very mildly on the input [Fe/H] and log g of each star (adopted from SSPP in our case) and it uses so many photometric bands that it relies very little on synthetic flux libraries – a claim that has been extensively tested in the literature (e.g. Blackwell, Petford & Shallis 1980; Alonso, Arribas & Martinez-Roger 1995; Casagrande, Portinari & Flynn 2006). In Fig. 7, we compare, for each star, the empirical BCs derived in the *ugriz* and JHK_S systems when using $f_{\rm Bol}$ from the IRFM, or as obtained instead by interpolating in our grids of MARCS synthetic photometry at the [Fe/H], log (from SSPP) and $T_{\rm eff}$ (from the IRFM) of each star.

This comparison allows us to easily quantify the performance of the MARCS synthetic fluxes in predicting broad-band colours on a star-by-star basis. In fact, it follows from equation (11) that a difference of Δ_ζ mag in a BC corresponds to a fractional uncertainty of $10^{-0.4\Delta_\zeta}$ in the derived bolometric flux. The BCs calculated from MARCS models usually agree to within 0.02 ± 0.07 mag with the values determined empirically from the IRFM for large ranges of $T_{\rm eff}$, [Fe/H], and log . Only in the u band is the uncertainty larger, and it shows systematic deviations towards the lowest surface gravities. The above numbers translate into a typical uncertainty of about 2 ± 7 per cent in the bolometric fluxes that are obtained from the MARCS tables. It should also be kept in mind that $f_{\rm Bol}$ values from the IRFM typically have errors of a few per cent. Overall, this implies that the grid of MARCS synthetic broad-band colours reported here can be used to reconstruct the bolometric flux of a star of known $T_{\rm eff}$, log g, and [Fe/H] to within an accuracy of a few per cent, and with a precision comparable to what can be achieved with empirical approaches. Also, the comparisons presented in Fig. 7 for a wide range of physical parameters in the *ugrizJHK_S* system is representative of the wavelength domain explored in this work, and of the parameter space covered by the MARCS library as a whole.

4.2 Colour–$T_{\rm eff}$–metallicity relations

Empirical colour–$T_{\rm eff}$–metallicity relations offer another way to test how well the interplay among these quantities is reproduced by
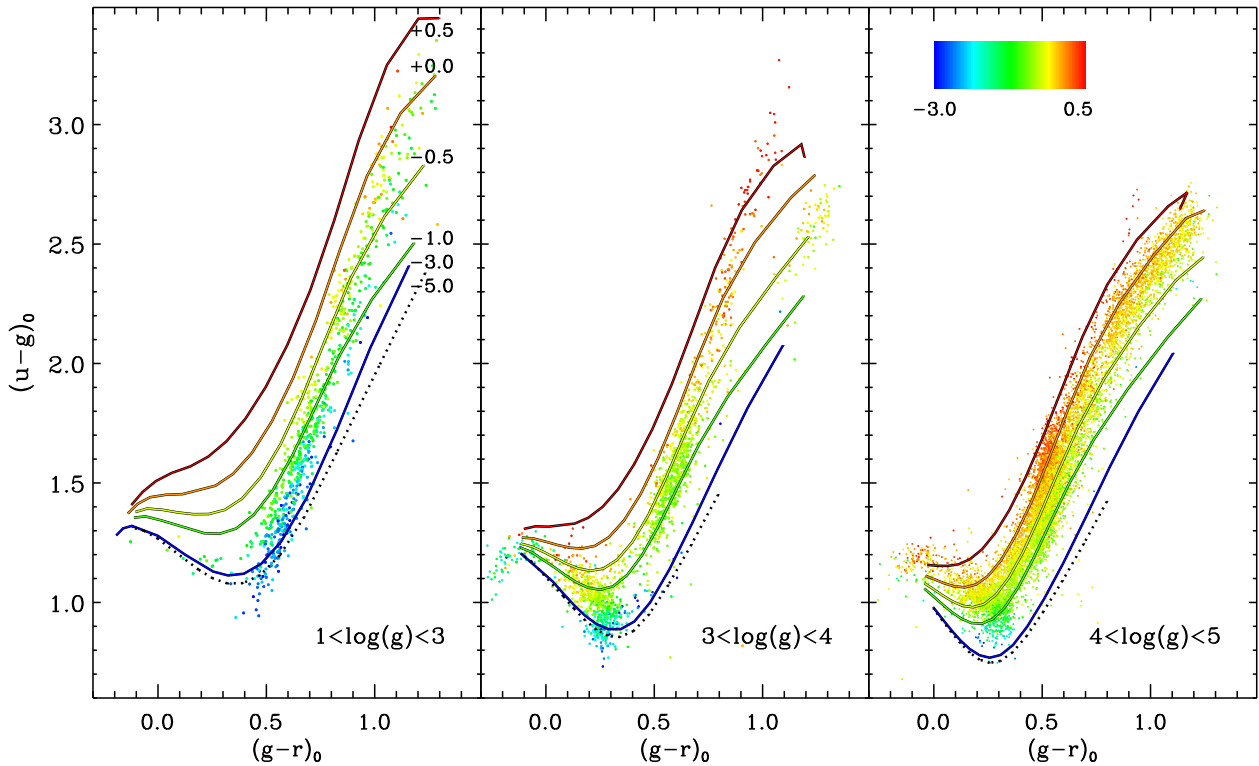
Figure 6. Comparison between observed and synthetic *ugriz* colours (α-standard, continuous lines) for a sample of about 13 500 stars in SEGUE DR8. Stars are dereddened using $E(B-V)$ values provided by SEGUE, sorted into panels according to surface gravity, and colour coded by metallicity (log g and [Fe/H] from the SSPP pipeline). MARCS (α-standard) colours are shown for fixed [Fe/H] from −5.0 to +0.5 (as indicated) and log $g = 2$ (left), 3.5 (centre) and 4.5 (right-hand panel), for $T_{eff} \geq 4000$ K.

synthetic flux models – before we 'attach' them to stellar isochrones (the subject of Section 4.3.) Using the routines described in Appendix A, we generated BCs in the BVI_CJK_S system (from which colour indices in any combination of the above filters can be derived) for two metallicities, [Fe/H] = 0.0 and −2.5, and T_{eff} values from 4500 K to 6500 K, in steps of 100 K, at two fixed values of log $g = 4.0$ and 4.5. These choices broadly encompass the properties of most of the subgiants and dwarf stars in the Galaxy.

For a fixed log g, we can then produce synthetic colour–T_{eff}–metallicity relations to be compared with the polynomials given by Casagrande et al. (2010): such comparisons are presented in Fig. 8. The empirical relations have a 'built-in' surface gravity dependence as they are valid for MS and subgiant stars. As a consequence, we chose to generate synthetic colours for values of T_{eff}, [Fe/H], and log g that are representative of the majority of the stars on which the empirical polynomials are based to do a better sampling of the parameter space which contains the observed stars. Fig. 8 shows the effect of using two different gravities mainly to demonstrate that the exact choice of log g is not the dominant factor in this comparison.

It is also worth noticing that the absolute calibration, zero-points, and filter transmission curves used in Casagrande et al. (2010) to derive the empirical relations closely match those used to produce synthetic MARCS BCs in this study (see Section 2.9). The comparisons performed here are thus largely free from any systematic biases that the above choices could introduce, and thus allows us to directly assess the degree to which the synthetic fluxes are able to match empirical relations. Overall, synthetic colours reproduce the main trends that are seen in empirical relations, as well as the crossing-over of the fiducial sequences for different values of [Fe/H] in certain colour indices. The agreement is particularly good around

5500 K in all of the colour indices which are examined in Fig. 8. The largest offsets are found for the $B - V$ colour index at lower temperatures and higher metallicities – which is not too surprising, considering the increased crowding of molecular lines in metal-rich dwarfs. Similarly, the predicted $J - K_S$ colours that we have derived from hot metal-rich ($T_{eff} \gtrsim 6000$ K) and cool metal-poor ($T_{eff} \lesssim 5200$ K) models increasingly depart from the empirical relations. In this case, however, it should be kept in mind that the scatter around the empirical $J - K_S$ relation is quite large, partly stemming from its limited colour baseline, and that it seems to underestimate T_{eff} above 6000 K (Pinsonneault et al. 2012). Nevertheless, all things considered, the comparisons given in Fig. 8 validate the MARCS effective temperature scale (for dwarfs and subgiants, in particular) when using indices such as $V - I_C$ or $V - K_S$, which have been shown to agree with the empirical Casagrande et al. (2010) scale, typically to much better than 100 K.

4.3 Open and globular clusters

Comparisons of computed isochrones with the observed CMDs of star clusters provide valuable tests of the consistency of synthetic colour–T_{eff} relations because the same interpretation of the data should be obtained on all CMDs. This is not to say that the models must provide perfect reproductions of the observed morphologies, but rather that whatever discrepancies exist between theory and observations in one CMD should be consistent with those that are apparent on other colour–magnitude planes. When that is not the case, this information can be used to pinpoint where inaccuracies occur in synthetic fluxes. To illustrate this, we have opted to consider the extensively studied globular cluster M 5, which has
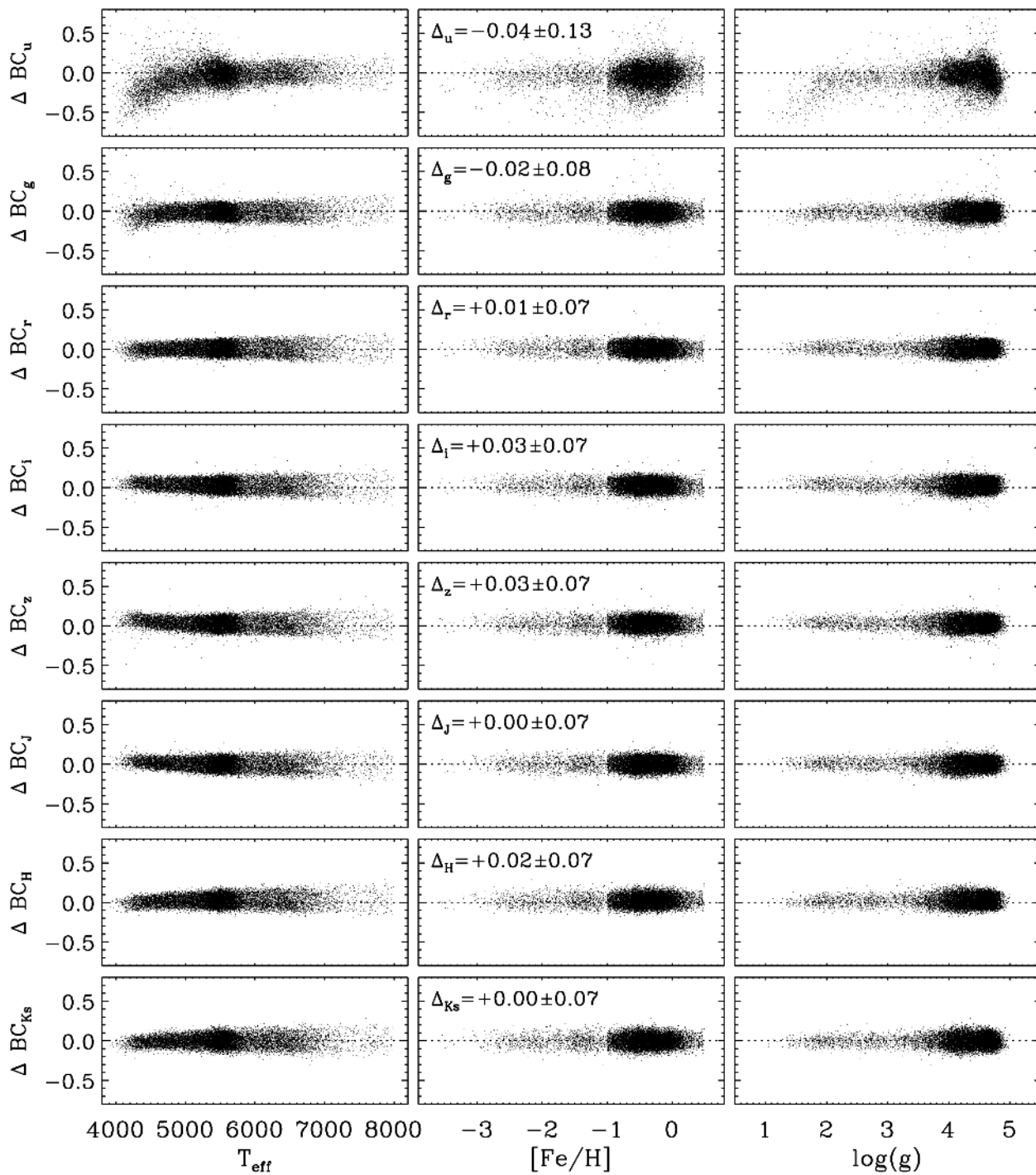
Figure 7. Comparison between empirical and MARCS (α-standard) BCs for stars in the previous Figure. For each band, the mean difference and the standard deviation are reported in the central panel.

[Fe/H] $= -1.33$ according to Carretta et al. (2009), the old, super-metal-rich open cluster NGC 6791 ([Fe/H] $\approx +0.3$; see Brogaard et al. 2012), and the near-solar-metallicity open cluster M 67. (It should be appreciated that some discrepancies between predicted and observed CMDs in an absolute sense will generally be present due to the uncertainties associated with, e.g. the treatment of convection and the atmospheric boundary conditions in stellar models, as well as those connected with the photometric data and such basic

cluster properties as the distance, reddening, and chemical abundances.)

In what follows, observations of these three systems are compared with the latest Victoria-Regina isochrones (VandenBerg et al. 2014) on several different CMDs. Rather than correcting the photometry for the effects of reddening and distance to obtain the intrinsic colours and absolute magnitudes, the model luminosities and temperatures have been converted to the *observed* magnitudes
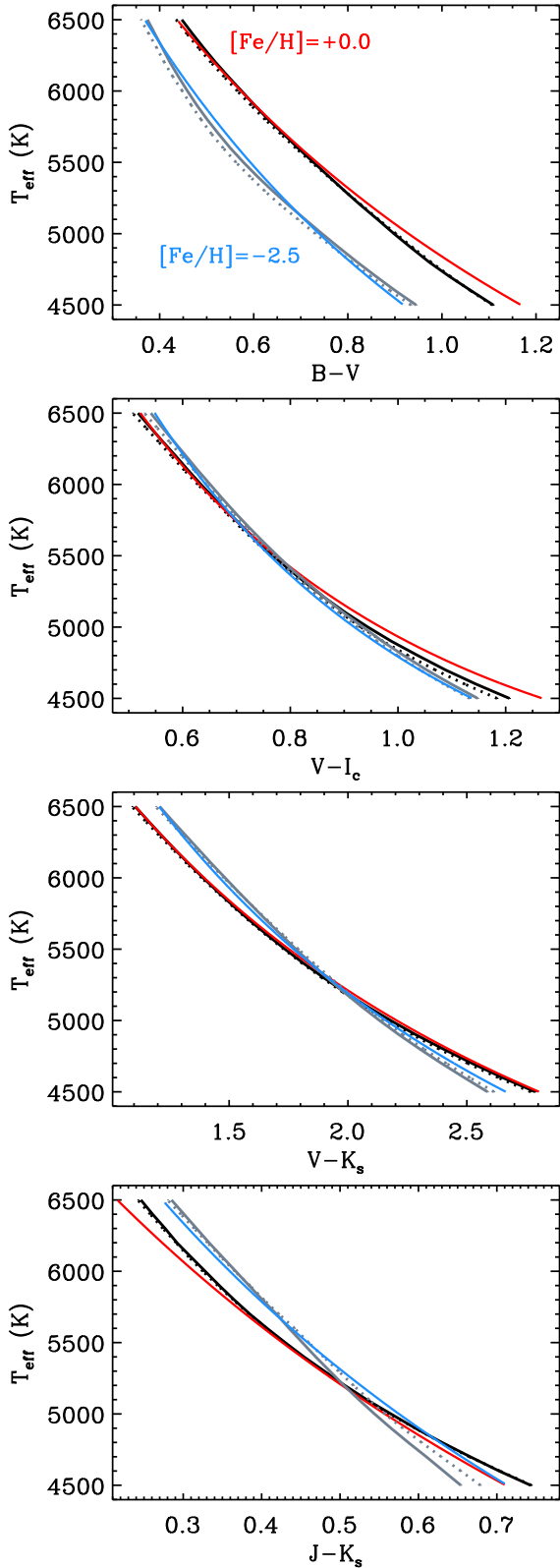
Figure 8. Comparison between the empirical colour–T_{eff}–metallicity relations of Casagrande et al. 2010 ([Fe/H] = 0.0 red, [Fe/H] = −2.5 blue), and those obtained from the MARCS (α-standard) fluxes at the same metallicity ([Fe/H] = 0.0 black, [Fe/H] = −2.5 grey) for two different gravities, log g = 4.0 (dotted line) and 4.5 (continuous line).

and colours using the reddening-adjusted transformations presented in this investigation. To accomplish this, values of $(m − M)_0$ (true distance moduli) that agree well with published estimates have been assumed. In all instances, well-supported determinations of the metallicity have been adopted, along with $E(B − V)$ values from Schlafly & Finkbeiner (2011, hereafter SF11), except in the case of NGC 6791. For this cluster, a slightly higher reddening, by ≈0.02 mag, appears to result in improved consistency over most of the colour planes that have been considered (see also discussion in Section 5, though it may instead be the assumed [Fe/H] value that is not quite right). Such issues are not of particular importance for the present analysis, however, as our primary goal is to study how the *differences* between the isochrones and the cluster CMDs vary with the particular colour index that has been plotted.

4.3.1 M 5 (NGC 5904)

Thanks to the efforts of P. B. Stetson, very high-quality, homogeneous Johnson–Cousins $BV(RI)_C$ photometry is available for relatively large samples of stars in many open and globular clusters (Stetson 2005). For a few of them, including M 5, U-band data may also be obtained from his 'Photometric Standard Fields' archive at the Canadian Astronomy Data Centre.[14] Indeed, his observations yield exceedingly tight, well-defined CMDs for M 5 from the tip of the RGB to ~2 mag below the TO. A further reason for choosing to use this system to examine the colour transformations for metal-poor stars is that it is nearly unreddened [$E(B − V) = 0.032$ according to SF11].

Fig. 9 plots the measured V magnitudes of the stars in the observed fields of M 5 as a function of their $U − B$, $B − V$, and $B − R_C$ colours. The solid curve in each panel is an 11.75 Gyr (VandenBerg et al. 2013) isochrone for [Fe/H] = −1.33, [α/Fe] = 0.4, and a helium abundance $Y = 0.25$. To place it on the observed planes, the so-called ubvri12 transformations for $E(B − V) = 0.032$ were used, together with $(m − M)_0 = 14.35$. Dashed loci represent the same isochrone, except that the ubvri90 transformations have been employed: differences between them and the solid curves are apparent only in the left-hand panel. Historically, synthetic $U − B$ colours have not been very reliable, but those based on the latest MARCS model atmospheres appear to be quite good (if the metallicity and distance that we have assumed for M 5 are accurate). Indeed, if the predicted $U − B$ colours were adjusted to the blue by only 0.02–0.03 mag, the isochrone would provide reasonably consistent fits to the observations on all three of the CMDs that are shown in Fig. 9. That is, independently of the colour that is considered, the isochrone would match the TO photometry satisfactorily and be somewhat too red along the RGB – except at $V \lesssim 15$ on the $(U − B, V)$-diagram, which suggests that the $U − B$ colours become less trustworthy at low gravities and/or cool temperatures. This is also in agreement to what was shown in Fig. 7 for the u filter.

The left-hand panel of Fig. 10 shows that the same consistency is found on the $(V − I_C, V)$-plane. Interestingly, this plot indicates a slight preference for the ubvri12 transformations to $V − I_C$ over those that we have labelled ubvri90, though this result will depend on the model T_{eff} scale, which is subject to many uncertainties. On the other hand, one would not expect to find such good agreement between the predicted and observed RGB morphologies unless the temperatures along the isochrones are quite close to those implied by the MARCS colour–T_{eff} relations. As illustrated in the right-hand

---

[14] See www1.cadc-ccda.hia-iha.nrc-cnrc.gc.ca/community/STETSON/

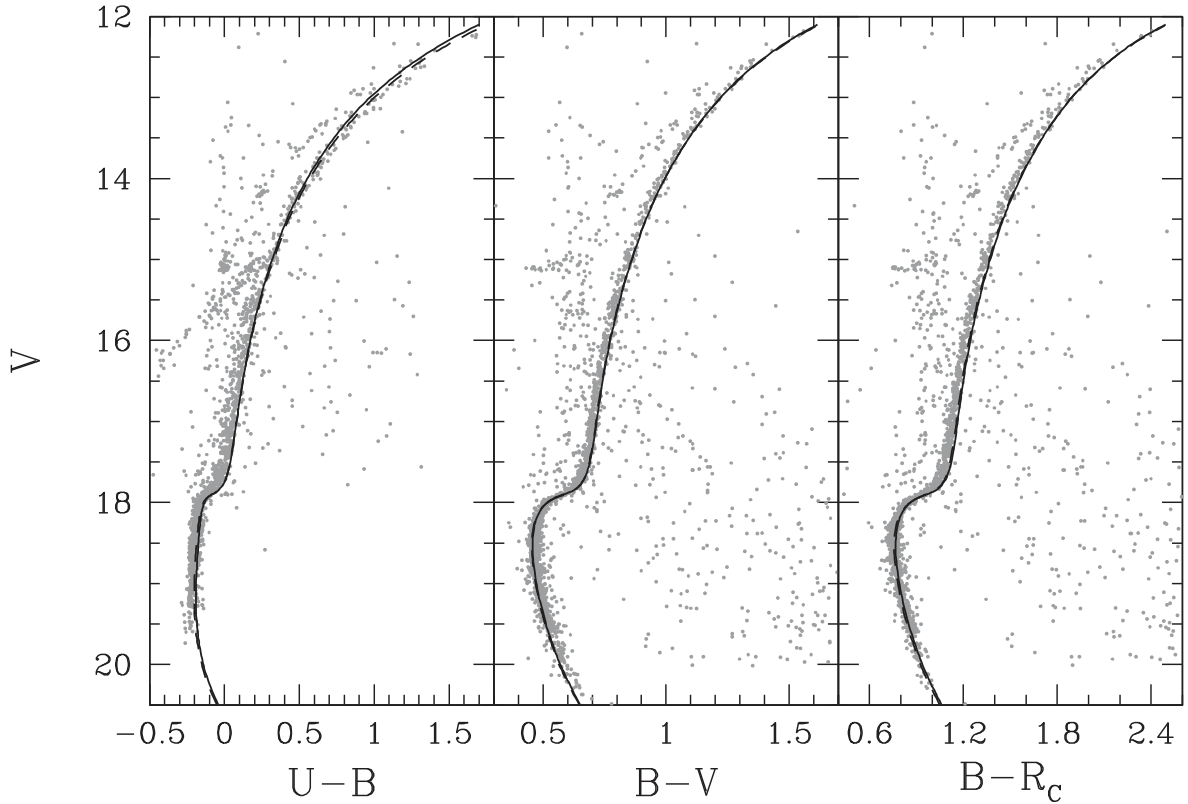**Figure 9.** Overlay of an 11.75 Gyr isochrone for [Fe/H] $= -1.33$, [α/Fe] $= 0.4$, and $Y = 0.25$ on to three CMDs of M 5 (see the text for the sources of the stellar models and the photometry). The solid and dashed curves assume the reddening-adjusted `ubvri12` and `ubvri90` colour transformations, respectively, for $E(B - V) = 0.032$ (from SF11). The true distance modulus of M 5 has been assumed to be $(m - M)_0 = 14.35$.
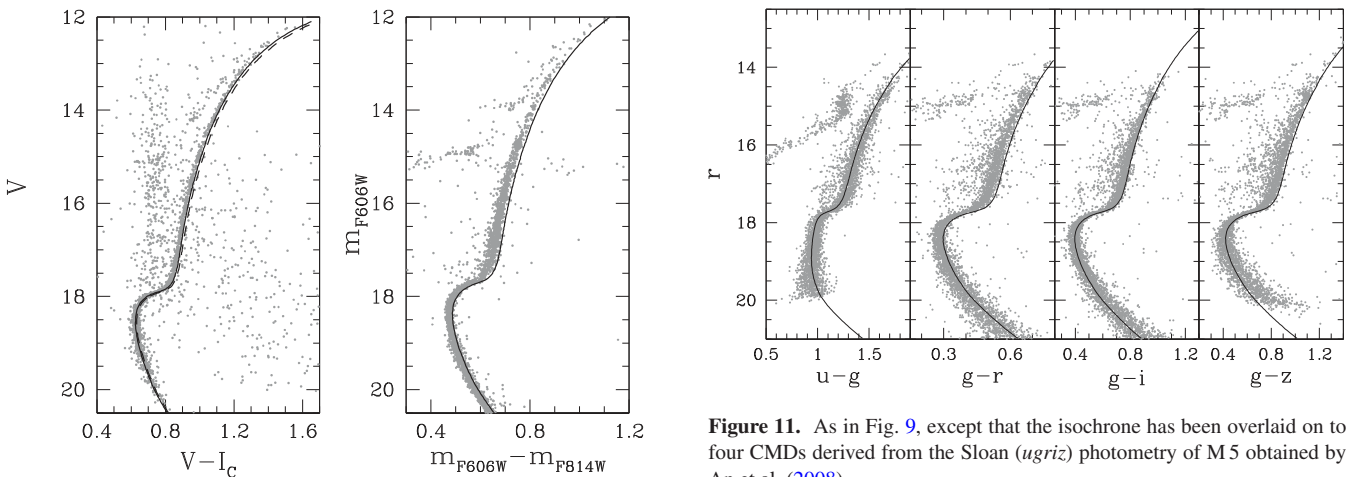

Figure 10. The left-hand panel extends the plots in the previous figure to the $(V - I_C, V)$-diagram. In the right-hand panel, *HST* ACS data for M 5 from Sarajedini et al. (2007) have been plotted, and the isochrone has been converted to the observed plane using the relevant transformations in the `VEGA-MAG` system (see Appendix A).

Figure 11. As in Fig. 9, except that the isochrone has been overlaid on to four CMDs derived from the Sloan (*ugriz*) photometry of M 5 obtained by An et al. (2008).

panel, very similar results are obtained when the same isochrone is compared with the *HST* ACS observations of M 5 that were obtained by Sarajedini et al. (2007). However, in this case, the isochrone does not match the observations quite as well as in the left-hand panel: to achieve a fully consistent fit, the models would need to be adjusted to the blue by 0.01–0.015 mag. It is not clear whether this zero-point

correction should be made to the colour transformations or to the photometric data (from either source).

The availability of Sloan (*ugriz*) observations of M 5 by An et al. (2008) gives us the opportunity to extend our comparisons to this photometric system. Four of the many possible CMDs that could be constructed from their observations are shown in Fig. 11, along with the same isochrone that has been plotted in the two previous figures, on the assumption of the same reddening and true distance modulus, etc. The fits to the data on the *g–i* and *g–z* colour planes closely resemble the fits to the $BV(RI)_C$ observations discussed above, which

implies satisfactory consistency between them. However, as in the case of the ACS photometry of M 5, the isochrone lies ∼0.02 to the red of the cluster MS and TO on the $(g - r, r)$-diagram, while it reproduces the observed $u - g$ colours (in the mean) for both the MS and RGB nearly perfectly. To try to identify whether the g or r magnitudes are primarily responsible for the offset in the $g - r$ colours, we produced a plot on the $(r - i, r)$-plane (not shown). It revealed that the isochrone is too blue relative to the observed TO by about 0.02 mag, from which we conclude that the difficulty with the $g - r$ colours is mainly due to a small problem with the r magnitudes. Whether this should be attributed to our transformations or to the observations, or both, is not known.

To improve our understanding of star clusters and of the photometric systems that are used, it is clearly advantageous to obtain observations through as many filters as possible. Encouragingly, most of the plots that we have produced for M 5 contain basically the same fit of the selected isochrone to the observations. In other words, the models generally provide a consistent interpretation of the data, regardless of the particular CMD that is considered. However, we did find a few 'exceptions to the rule', which is to be expected given the difficulty of establishing the zero-points of synthetic or observed photometry to within ∼0.01–0.02 mag and the uncertainties associated with current model atmospheres and synthetic spectra. In fact, the small colour offsets that we found on some colour–magnitude planes may also be a reflection of the assumed metal abundances; i.e. perhaps improved overall consistency would have been obtained had our analysis used stellar models that assumed a different mixture of the heavy elements. Although it is beyond the scope of the present investigation to do so, this possibility should be fully explored.

4.3.2 NGC 6791

Brogaard et al. (2011, 2012) have carried out the most exhaustive studies of NGC 6791 to date, finding an age of 8–8.5 Gyr if $Y \approx 0.30$ and [Fe/H] = 0.30–0.35, when fits of stellar models to the mass–radius diagrams of the binaries known as V18 and V20 are taken into account. Their results are based predominantly on isochrones that assume the solar mix of the heavy elements as reported by Grevesse & Sauval (1998), suitably scaled to the [Fe/H] values of interest. For this work, which uses the latest Victoria-Regina isochrones (VandenBerg et al. 2014), the updated solar abundances by Asplund et al. (2009) provide the reference metals mixture. According to VandenBerg et al., their models require $Y \approx 0.28$ to satisfy the same binary constraints if NGC 6791 has [Fe/H] = 0.30 – and we have therefore adopted these estimates of the helium and metallicity.

Unfortunately, the reddening of NGC 6791 has been particularly hard to pin down. The value of $E(B - V) = 0.155$ from the original Schlegel et al. (1998) dust maps has been revised downwards to 0.133 mag by SF11. Moreover, as discussed by Brogaard et al. (2012), who concluded that the current best estimate of the reddening is 0.14 ± 0.02, it appears to be difficult to obtain consistent fits to the $(B - V, V)$- and $(V - I_C, V)$-diagrams unless a small systematic shift is applied to one of the predicted colours. Part of the difficulty, as noted by them, is that the value of $E(V - I_C)/E(B - V)$ appears to be uncertain (e.g. Hendricks et al. 2012, their tables 11–13). As it turns out, it *is* possible to obtain nearly indistinguishable fits of isochrones to observations of NGC 6791 on many different CMDs (using our predictions for the effects of reddening on the synthetic magnitudes and colours) if the cluster has $E(B - V) = 0.16$.
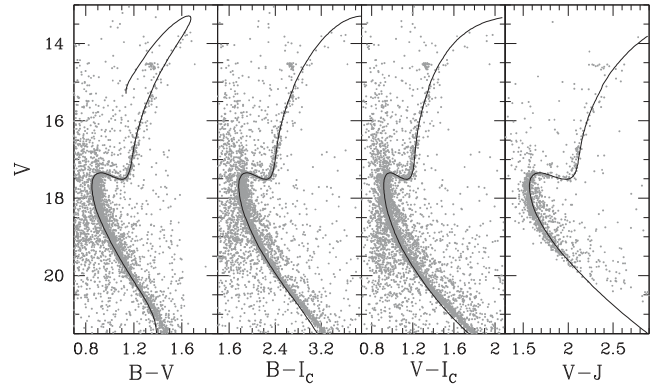

Figure 12. Overlay of an 8.5 Gyr isochrone for [Fe/H] =+0.30, [α/Fe] =0.0, and $Y = 0.28$ on to four CMDs of NGC 6791 (see the text for the sources of the stellar models and the observations). The solid curves assume the reddening-adjusted `ubvri12` and the SDSS J transformations for $E(B - V) = 0.16$. The true distance modulus of NGC 6791 has been assumed to be $(m - M)_0 = 13.05$.
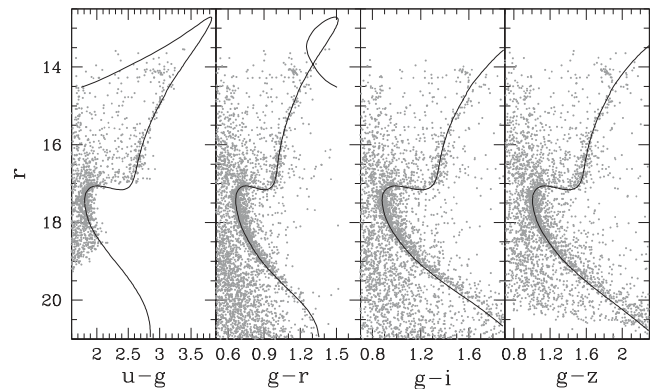

Figure 13. As in the previous figure, except that the isochrone has been overlaid on to four CMDs derived from the Sloan (*ugriz*) photometry of NGC 6791 obtained by An et al. (2008).

This is shown in Figs 12 and 13 where, in turn, an 8.5 Gyr isochrone for the aforementioned chemical abundances has been overlaid on to a number of CMDs derived from BVI_CJ and *ugriz* photometry of NGC 6791. All fits assume $(m - M)_0 = 13.05$. The BVI_C photometry that we have used is contained in the `NGC6791.KFB` and `NGC6791.COR` files that can be downloaded from the 'Homogeneous Photometry link at the same CADC website address (see footnote 14) that was used to obtain the M 5 data. Although *U*-band observations are not available, we have been able to extend our comparisons to the near-IR by adding a panel that plots the Johnson V, 2MASS J photometry from Brasseur et al. (2010). For whatever reason, the isochrone lies along the red edge of the distribution of MS stars on the $(V - J, V)$-diagram, while it coincides closely with the blue edge in the other panels, as well as in at least three of the four CMDs shown in Fig. 13. [The isochrone appears to match the mean MS fiducial on the $(u - g, r)$-plane, but the TO is close to the limit of the *u* photometry.] As in the case of M 5, the Sloan photometry of NGC 6791 that we have used has been taken from An et al. (2008).

Even in an absolute sense, the isochrone clearly reproduces the observed CMDs of NGC 6791 rather well from 3–4 mag below the TO to approximately the luminosity of the horizontal branch clump.

At higher luminosities, the predicted colours tend to be too blue, indicating a problem with either the MARCS transformations or the model temperatures or both. (For quite a thorough discussion of this issue, reference may be made to VandenBerg et al. 2014.) Although Figs 12 and 13 appear to provide compelling support for the derived (or adopted) properties of NGC 6791, we have not explored whether equally good fits of the isochrones to the observed CMDs (and the cluster binaries) can be obtained for different combinations of [Fe/H], the mix of heavy elements, Y, $E(B - V)$, $(m - M)_0$, and age. This would be well worth investigating. Note that the unusual morphology of the upper RGB portion of the isochrone in the $(B - V, V)$-, $(u - g, r)$-, and $(g - r, r)$-diagrams is consistent with the predicted behaviour of the synthetic magnitudes in the respective filters, and are not a consequence of, say, extrapolations in the colour transformation tables. On the other hand, that morphology will be a sensitive function of the model T_{eff} scale; i.e. if the predicted RGB were appreciably cooler or hotter, the blueward excursion of upper RGB in the left-hand panel of Fig. 13 and the loop in the adjacent panel would be accentuated or minimized.

4.3.3 M 67 (NGC 2682)

Our emphasis thus far has been on upper MS and more evolved stars because several recent papers have already shown that the slope of the MS down to $M_V \sim 7$–8 in open and globular clusters and as defined by local subdwarfs, over a wide range in [Fe/H], can be reproduced quite well by stellar models that employ the MARCS colour transformations (see Brasseur et al. 2010; VandenBerg et al. 2010, 2013, 2014). Hence, for our final comparisons of isochrones with cluster observations, we decided to focus on the lower MS extension of M 67, given that *ugriz* (An et al. 2008) and BVI_CJK_S photometry is available for low-mass stars belonging to this system. [The 2MASS observations (Skrutskie et al. 2006) were kindly provided to us by A. Dotter (see Sarajedini, Dotter & Kirkpatrick 2009), while the Johnson–Cousins photometry is from the same CADC website mentioned previously (see footnote 14).]

In Figs 14 and 15, eight of the possible CMDs that can be produced from these data have been superimposed by the MS segment of the same 4.3 Gyr, [Fe/H] = 0.0 (e.g. Randich et al. 2006, Önehag et al. 2011), $Y = 0.255$ isochrone that was compared with observations for the upper MS and RGB stars of M 67 by VandenBerg
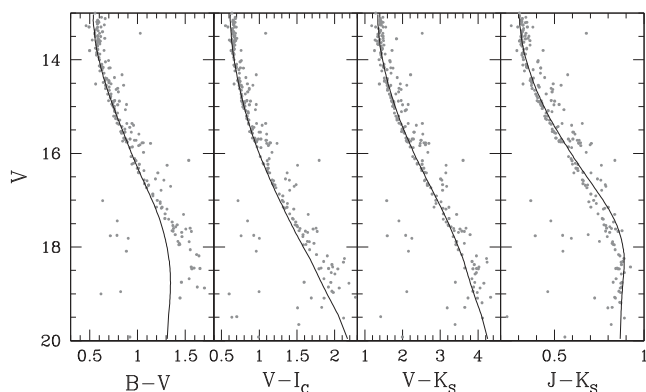

Figure 14. Overlay of the lower MS portion of a 4.3 Gyr isochrone for [Fe/H] =0.0, [α/Fe] =0.0, and $Y = 0.255$ on to four CMDs for MS stars in M 67 (see the text for the sources of the stellar models and the observations). The solid curves assume the reddening-adjusted `ubvri12` and the SDSS JK_S transformations for $E(B - V) = 0.030$. The true distance modulus of M 67 has been assumed to be $(m - M)_0 = 9.60$.
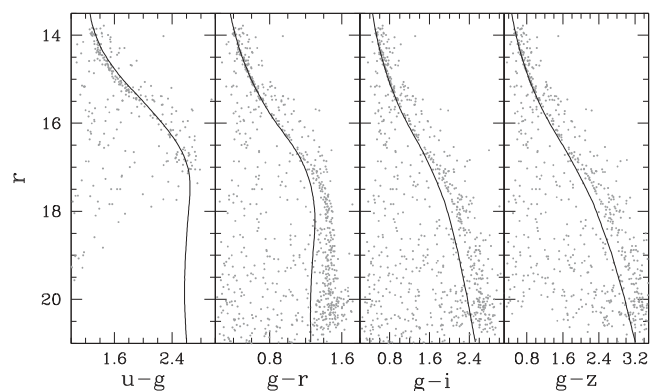

Figure 15. As in the previous figure, except that the isochrone has been overlaid on to four CMDs derived from the Sloan (*ugriz*) photometry of M 67 obtained by An et al. (2008).

et al. (2014). In all cases, $E(B - V) = 0.030$ (SF11) and $(m - M)_0 = 9.60$ has been assumed. Except for the $J–K_S$ and $u–g$ colour planes, the isochrone matches the MS stars that have V (or r) $\lesssim$ 17 very well. As expected, the observed $B - V$ colours of cool, faint stars are more problematic than their $V - K_S$ colours. Indeed, the close agreement of the isochrone with the observations on the $(V - K_S, V)$-diagram suggests that the temperatures of the models are quite good (for additional discussion of this issue see Vanden-Berg et al. 2014). If this is correct, then the deviations which are apparent at faint magnitudes in the other CMDs must be telling us something about the MARCS transformations, or the photometric data, or perhaps that the assumed metallicity or metals mixture is wrong. As discussed in the next section, colours for metal-rich, lower MS stars are especially dependent on [Fe/H] and [α/Fe] (and presumably on any metal with a high abundance). (We note, in closing this section, that fits of completely independent isochrones to the Sloan data for M 67 were obtained by An et al. 2009.)

5 MORPHOLOGY OF THE CMD IN VARIOUS COLOUR PLANES AND AS FUNCTION OF REDDENING

With our set of stellar isochrones and colours, it is of some interest to study how variations in chemical composition – [α/Fe], to be specific – affect the morphology of the CMD when using different filter combinations. For this purpose, we consider two different cases. In Fig. 16, we examine the effects of changing the α-element abundances on the location and shape of an [Fe/H] = −0.8, 12 Gyr isochrone, which is roughly representative of moderately metal-rich globular clusters in the Milky Way. The upper left-hand panel shows three isochrones in the theoretical $\log T_{eff}$–M_{Bol} diagram, all for the same iron content, but different values of [α/Fe]. Because of this difference, the total mass-fraction abundance of the metals (Z) is somewhat different in the three isochrones, which explains why they are slightly offset from each other. However, apart from this, there are no morphological changes.

The other panels of Fig. 16 show the same three isochrones, but as transformed to various CMDs that involve the magnitudes predicted for various optical and IR filters. In nearly all cases, the only part of the CMD that is substantially affected by variations in the abundances of the α-elements is the lower MS (at $T_{eff} \lesssim$ 4000 K). A detailed explanation of the cause(s) of this sensitivity is beyond the scope of this paper, but it stems essentially from the onset of various molecules (e.g. H_2O and TiO, which form
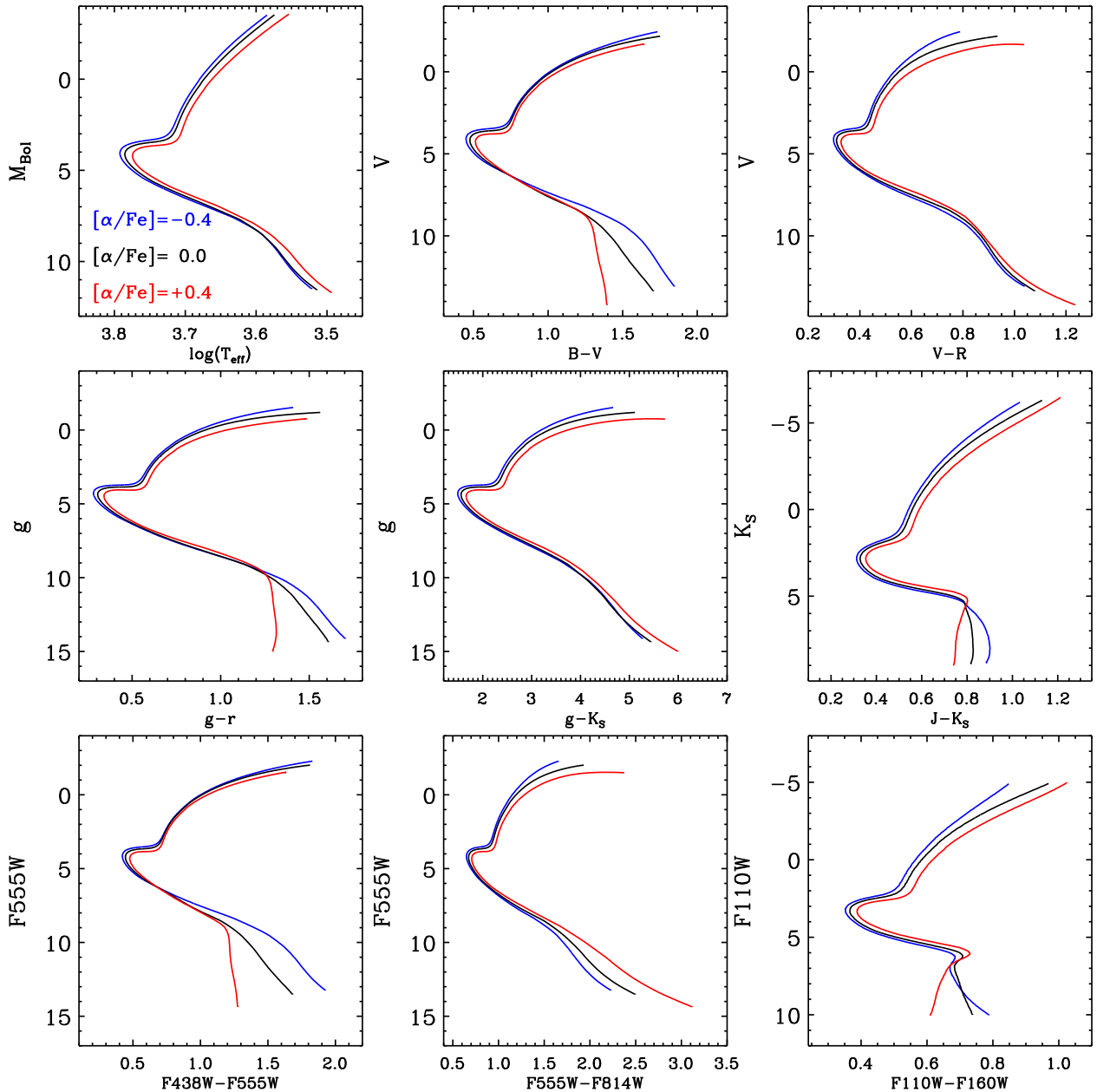
Figure 16. Morphology of the CMD in different combinations of filters for a 12 Gyr isochrone having $Y = 0.25$, $[Fe/H] = -0.8$, and three different values of $[\alpha/Fe] = -0.4, 0,$ and $+0.4$.

more easily with increasing $[\alpha/Fe]$) as important sources of blanketing. Interestingly, recent $F110W$ and $F160W$ photometry of two globular clusters (namely, NGC 2808 and M 4, which both have $[Fe/H] \simeq -1.2$; e.g. Carretta et al. 2009, making them about 0.4 dex more metal-poor than the isochrones considered here) has revealed that they have split lower MSs (Milone et al. 2012, 2014). Indeed, the observed morphologies are qualitatively quite similar to the results shown in the bottom right-hand panel, which suggests that star-to-star variations in the abundances of one or more of the α-elements is responsible for this phenomenon. It may be the case, for instance, that a split MS is one of the consequences of the presence of O-rich and O-poor populations within a given globular cluster. Further work is clearly needed to check out this speculation, but the main point of this example is that chemical abundance anomalies can be expected to leave detectable photometric signatures.

Fig. 17 is identical to the previous one (in particular, the same variations of $[\alpha/Fe]$ are considered), except that somewhat younger isochrones (10 Gyr) for $[Fe/H] = 0.0$ have been plotted. The split in the lower MS is even more dramatic, and certain filter combinations reveal interesting features for the upper CMD (above the TO) as well. As the abundances of the α-elements increase, the RGB swings to blue and red colours and even makes loops in the CMD in some cases. Again, a detailed discussion of the causes of such effects is beyond our purposes, but a visual inspection of synthetic RGB optical spectra provides a clue as to what is going on. At low α-element abundances ($[\alpha/Fe] = -0.4$), the overall shapes of spectra essentially scale with decreasing T_{eff} (implying that, e.g. the $g - r$ index gets monotonically redder). However, in the α-enhanced models, there is a dramatic dampening of the flux with decreasing T_{eff}, likely driven by the strengthening TiO bandheads. We suspect
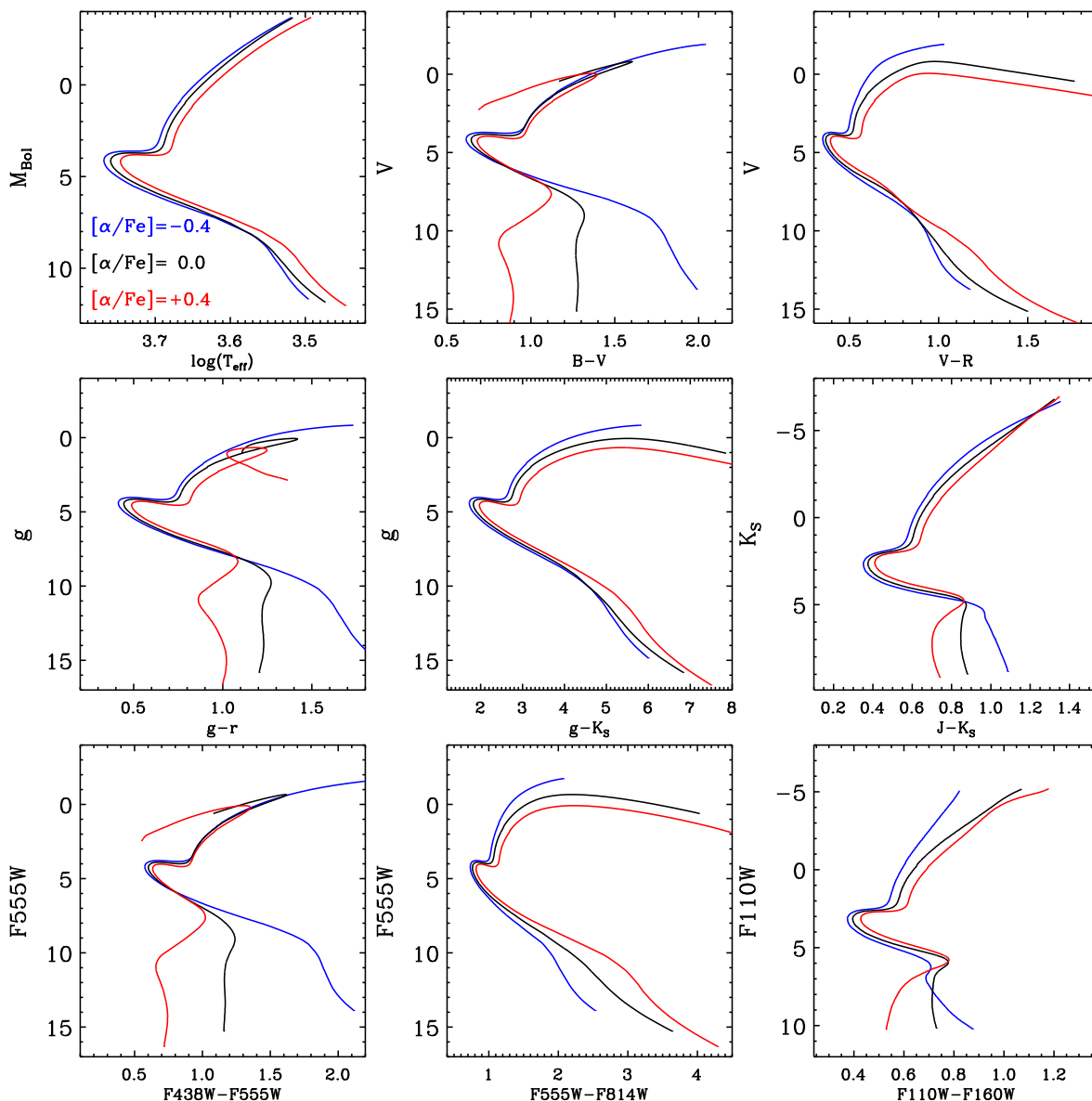
Figure 17. Same as previous Figure, but using instead a 10 Gyr isochrone having $Y = 0.25$ and [Fe/H] = 0.0.

that this prevents some colour indices from getting monotonically redder with decreasing $T_{\rm eff}$.

While we defer a more detailed explanation of these effects to a subsequent investigation, optical spectrophotometry of cool metal-rich giants (e.g. the Next Generation Spectral Library; Heap & Lindler 2010, and the Medium Resolution INT Library of Empirical Spectra; Sánchez-Blázquez et al. 2006) can be used to assess the reliability of synthetic spectra in this regime. Nevertheless, the apparent high sensitivity of many colours to the temperatures and chemical abundances of metal-rich stars (both of giants and dwarfs, depending on the filters used) has considerable potential in advancing our understanding of, in particular, the Galactic bulge given that it may be possible to distinguish between α-rich and -poor populations.

Our final topic of discussion concerns the effects of extinction on the CMD. In most investigations, the extinction coefficient in a given band R_ζ is assumed to be constant for stars of different spectral types. That is, once a value of $E(B - V)$ is known, the colour excess

in any colour other than $B - V$ is determined from $E(\zeta - \eta) = A_\zeta - A_\eta = (R_\zeta - R_\eta)E(B - V)$, from which the unreddened colour index is

$$(\zeta - \eta)_0 = (\zeta - \eta) - E(\zeta - \eta). \tag{20}$$

Similarly, for magnitudes

$$m_{\zeta,0} = m_\zeta - A_\zeta = m_\zeta - R_\zeta E(B - V), \tag{21}$$

and the distance modulus in a given band ζ (affected by extinction A_ζ) is related to the true distance modulus via $(m - M)_0 = (m - M)_\zeta - A_\zeta$. In Fig. 18, we show in red a metal-poor isochrone on different colour–magnitude planes that has been reddened at each point with an input $R_V = 3.1$ extinction law, assuming a nominal $E(B - V) = 0.6$. As discussed in Section 2.8, our nominal extinction coefficient and colour excess are valid for early-type stars. In panel (a), we show in green the same isochrone, but in this case the reddening has been calculated assuming the same colour excess (0.6) and $R_V = 3.1$ in the relations (20)–(21) above. Likewise, in panel
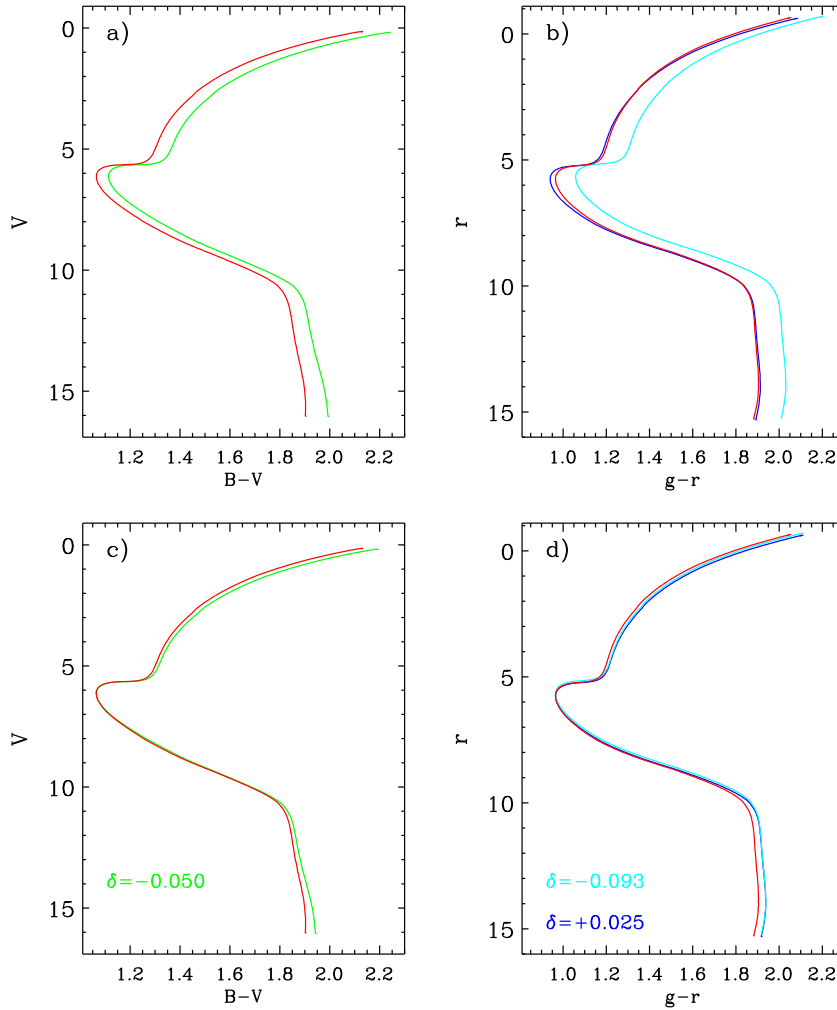
Figure 18. Effect of reddening $E(B - V) = 0.6$ on a 12 Gyr, $Y = 0.25$, [Fe/H] $= -0.8$, [α/Fe] $= +0.4$ isochrone when using our published colours (in red), or assuming constant extinction coefficients (green, blue and cyan). See text for discussion.

(b), we show the effect of using the constant SDSS extinction co-efficients provided by An et al. (2009, in blue) and McCall (2004, in cyan). The extinction coefficients of An et al. (2009) closely match the absolute position of our reddened isochrone, simply because those coefficients were derived using a synthetic spectrum for log $g = 4.5$, [Fe/H] $= 0.0$, and $T_{\rm eff} = 5750$ K, which is similar to those that are appropriate for our reference isochrone. In contrast, the extinction coefficients given by McCall (2004) were derived using the α Lyr reference spectrum, which is responsible for the relatively large offset between the cyan and red isochrones. These two panels thus illustrate the risk involved in trying to fit isochrones to photometric data on the assumption of a literature value of $E(B - V)$ when a slightly different value may actually be more correct for the stars under investigation.

In the lower panels (c) and (d), we re-register all of the isochrones to match our reference isochrone at the TO point, applying whatever colour shifts δ are required (as noted). Alternatively, it would be possible to obtain the same result using in the relations (20)–(21), the extinction and reddening coefficient appropriate for a moderately metal-poor TO star (i.e. $E(B - V) = 0.55$ and $R_V = 3.40$ for the case of panel (c) and $E(B - V) = 0.55$, $E(g - r) = 0.62$, and $R_r = 2.95$ for the case of panel (d), see Section 2.8 and Appendix A). Nevertheless, it is clear from these panels that, despite this renor-

malization, the morphologies of the CMDs for the different cases are not identical along the lower MS or the RGB. While these subtleties are usually negligible in the presence of low reddening, this is not the case for high values of the extinction. We emphasize that our reddened colours account for the effects of extinction in a fully self-consistent way. We also reiterate our comment that, when using literature values of $E(B - V)$, attention should be paid to how they were derived in order to minimize the inconsistencies highlighted above. More often than not, small adjustments to literature values of $E(B - V)$ might be applied. However, this should not be regarded as an excuse to use reddening as a free parameter, since an error in the reddening is only one of many possible reasons why an isochrone may not reproduce the observed TO colour of a cluster CMD even when well-supported estimates of the distance, metallicity, and $E(B - V)$ are adopted.

6 CONCLUSIONS

The large grids of MARCS model atmospheres, now available for different chemical compositions, together with the fluxes calculated at $\sim 10^5$ wavelength points, represent an especially valuable resource for the study of stars and stellar populations (Gustafsson et al. 2008). To facilitate their application to photometric data, we have provided

the means to generate, and to interpolate in, tables of synthetic BCs (and thus colours) applicable to several broad-band systems, for a wide range of physical and chemical abundance parameters (see Appendix A for detailed information on the parameter space covered). The photometric systems for which such transformations are provided include Johnson–Cousins-2MASS ($UBVR_CI_CJHK_S$), Sloan (*ugriz*), and *HST*-ACS/WFC3 (26 different filters, each in the ST, AB, and VEGA mag systems). The differences between the latter have been fully described, and the most updated photometric zero-points and absolute calibrations used. A novel feature of our transformations is that they can be corrected for the effects of reddening (for any $E(B - V)$ value between 0.0 and 0.72, inclusive) in a fully consistent way; i.e. the variation in the colour excess with the spectral type of a star is correctly taken into account. So far, our results assume the standard $R_V = 3.1$ for the extinction law, although the inclusion of other values (as e.g. more appropriate towards certain Galactic sightlines) is currently underway. The impact of varying the assumed microturbulent velocity on synthetic magnitudes in UV, optical, and IR bandpasses has also been examined in some detail: all of our results assume $\xi = 2 \text{ km s}^{-1}$. While this value is generally appropriate for stars across most of the CMD, its variation can seriously impact colours for $T_{\rm eff} \lesssim 4000\,\text{K}$, and increasing metallicities, in particular towards the UV.

Encouragingly, we have found that the MARCS colour–$T_{\rm eff}$–metallicity relations and BCs in most of the broad-band filters agree with those derived empirically above $\simeq 4500\,\text{K}$ using the IRFM (Casagrande et al. 2010) to within a couple/few per cent. This is easily within the uncertainties associated with the zero-points of the photometric systems and of the temperature scale. Moreover, the predicted metallicity dependence of such relations appears to reproduce observed trends quite well according to our analyses of a large sample of solar neighbourhood stars that have *ugriz* photometry. In general, the fits of isochrones to globular and open cluster CMDs (specifically, those of M 5, NGC 6791, and M 67) yielded consistent interpretations of the data on different colour planes, though small (0.01–0.02 mag) colour offsets were sometimes found in some CMDs relative to others for the same cluster. Even the synthetic *U* magnitudes did not appear to be seriously discrepant, at least for metal-poor TO stars. Larger deficiencies might affect synthetic colours of late M-stars, although this regime has only been partly explored in this work (and certainly not at the coolest $T_{\rm eff}$ of the MARCS grid).

Our brief consideration of Victoria-Regina isochrones on many different CMDs revealed the strong sensitivity of the colours of lower MS stars to [α/Fe], which undoubtedly has relevance for the bifurcated CMDs of M 4 and NGC 2808. Not surprisingly, the colours of cool stars, are very dependent on the chemical composition. As such, changing [α/Fe] can modify quite dramatically the morphology of the CMD at its coolest extremities, both along the lower MS and upper RGB.

We defer to a future investigation a more detailed exploration of the effects of chemical abundances on colours, in particular accounting for the anticorrelations observed in many globular clusters (e.g. Sbordone et al. 2011). In this respect, it will also be interesting to extend our grid of synthetic BCs to intermediate- and narrow-band systems, where synthetic models seem to perform less satisfactorily in comparison with observations (e.g. Önehag et al. 2009; Meléndez et al. 2010). The Strömgren system will also be of particular interest, because of its capability to help distinguish between multiple populations in globular clusters (e.g. Grundahl, Vandenberg & Andersen 1998; Yong et al. 2008; Carretta et al. 2011).

REFERENCES

Allende Prieto C., Barklem P. S., Lambert D. L., Cunha K., 2004, A&A, 420, 183
Aller L. H., 1963, Astrophysics. The Atmospheres of the Sun and Stars. Ronald Press, New York
Alonso A., Arribas S., Martinez-Roger C., 1995, A&A, 297, 197
Alonso A., Arribas S., Martinez-Roger C., 1996, A&A, 313, 873
An D. et al., 2008, ApJS, 179, 326
An D. et al., 2009, ApJ, 700, 523
Árnadóttir A. S., Feltzing S., Lundström I., 2010, A&A, 521, A40
Asplund M., Grevesse N., Sauval A. J., Scott P., 2009, ARA&A, 47, 481
Aumann H. H. et al., 1984, ApJ, 278, L23
Bedin L. R., Piotto G., Anderson J., Cassisi S., King I. R., Momany Y., Carraro G., 2004, ApJ, 605, L125
Beeck B., Cameron R. H., Reiners A., Schüssler M., 2013, A&A, 558, A48
Bell R. A., Gustafsson B., 1989, MNRAS, 236, 653
Bessell M. S., 1990a, A&AS, 83, 357
Bessell M. S., 1990b, PASP, 102, 1181
Bessell M. S., 2000, PASP, 112, 961
Bessell M. S., 2005, ARA&A, 43, 293
Bessell M. S., 2011, in Qain S., Leung K., Zhu L., Kwok S., eds, ASP Conf. Ser. Vol. 451, 9th Pacific Rim Conference on Stellar Astrophysics. Astron. Soc. Pac., San Francisco, p. 205
Bessell M., Murphy S., 2012, PASP, 124, 140
Bessell M. S., Castelli F., Plez B., 1998, A&A, 333, 231
Blackwell D. E., Petford A. D., Shallis M. J., 1980, A&A, 82, 249
Bohlin R. C., 2007, in Sterken C., ed., ASP Conf. Ser. Vol. 364, The Future of Photometric, Spectrophotometric and Polarimetric Standardization. Astron. Soc. Pac., San Francisco, p. 315
Bohlin R. C., 2010, AJ, 139, 1515
Bonnell J., Bell R. A., 1982, MNRAS, 201, 253
Brasseur C. M., Stetson P. B., VandenBerg D. A., Casagrande L., Bono G., Dall'Ora M., 2010, AJ, 140, 1672
Brogaard K., Bruntt H., Grundahl F., Clausen J. V., Frandsen S., Vandenberg D. A., Bedin L. R., 2011, A&A, 525, A2
Brogaard K. et al., 2012, A&A, 543, A106
Brott I., Hauschildt P. H., 2005, in Turon C., O'Flaherty K. S., Perryman M. A. C., eds, ESA SP-576: Proceedings of the Gaia Symposium: The Three-Dimensional Universe with Gaia. p. 565, ESA, Noordwijk
Cardelli J. A., Clayton G. C., Mathis J. S., 1989, ApJ, 345, 245
Carretta E., Bragaglia A., Gratton R., D'Orazi V., Lucatello S., 2009, A&A, 508, 695
Carretta E., Bragaglia A., Gratton R., D'Orazi V., Lucatello S., 2011, A&A, 535, A121
Casagrande L., 2009, Mem. Soc. Astron. Ital., 80, 727
Casagrande L., Portinari L., Flynn C., 2006, MNRAS, 373, 13
Casagrande L., Flynn C., Portinari L., Girardi L., Jimenez R., 2007, MNRAS, 382, 1516
Casagrande L., Ramírez I., Meléndez J., Bessell M., Asplund M., 2010, A&A, 512, A54
Casagrande L., Schönrich R., Asplund M., Cassisi S., Ramírez I., Meléndez J., Bensby T., Feltzing S., 2011, A&A, 530, A138
Casagrande L., Ramírez I., Meléndez J., Asplund M., 2012, ApJ, 761, 16
Casagrande L. et al., 2014a, MNRAS, 439, 2060

Casagrande L. et al., 2014b, ApJ, 787, 110
Castelli F., Kurucz R. L., 2004, preprint (astro-ph/0405087)
Clem J. L., VandenBerg D. A., Grundahl F., Bell R. A., 2004, AJ, 127, 1227
Cohen M., Wheaton W. A., Megeath S. T., 2003, AJ, 126, 1090
Edvardsson B., 2008, Phys. Scr. T, 133, 014011
Edvardsson B., Andersen J., Gustafsson B., Lambert D. L., Nissen P. E., Tomkin J., 1993, A&A, 275, 101
Eggen O. J., Lynden-Bell D., Sandage A. R., 1962, ApJ, 136, 748
Eisenstein D. J. et al., 2006, ApJS, 167, 40
Fitzpatrick E. L., 1999, PASP, 111, 63
Fuhrmann K., 2008, MNRAS, 384, 173
Fukugita M., Ichikawa T., Gunn J. E., Doi M., Shimasaku K., Schneider D. P., 1996, AJ, 111, 1748
Girardi L., Bertelli G., Bressan A., Chiosi C., Groenewegen M. A. T., Marigo P., Salasnich B., Weiss A., 2002, A&A, 391, 195
Girardi L., Grebel E. K., Odenkirchen M., Chiosi C., 2004, A&A, 422, 205
Golay M., 1972, Vistas Astron., 14, 13
Golay M., ed., 1974, Astrophysics and Space Science Library, Vol. 341, Introduction to Astronomical Photometry. Reidel, Dordrecht, p. 375
Gray R. O., Graham P. W., Hoyt S. R., 2001, AJ, 121, 2159
Grevesse N., Sauval A. J., 1998, Space Sci. Rev., 85, 161
Grevesse N., Asplund M., Sauval A. J., 2007, Space Sci. Rev., 130, 105
Grundahl F., Vandenberg D. A., Andersen M. I., 1998, ApJ, 500, L179
Gustafsson B., Edvardsson B., Eriksson K., Jørgensen U. G., Nordlund Å., Plez B., 2008, A&A, 486, 951
Harris W. E., Fitzgerald M. P., Reed B. C., 1981, PASP, 93, 507
Hayes D. S., Latham D. W., 1975, ApJ, 197, 593
Heap S. R., Lindler D., 2010, Bull. Am. Astron. Soc., 42, 463.02
Hendricks B., Stetson P. B., VandenBerg D. A., Dall'Ora M., 2012, AJ, 144, 25
Holberg J. B., Bergeron P., 2006, AJ, 132, 1221
Howell S. B., 1989, PASP, 101, 616
Ivezić Ž. et al., 2007, AJ, 134, 973
Ivezić Ž. et al., 2008, ApJ, 684, 287
Johnson H. L., 1966, ARA&A, 4, 193
Johnson H. L., Morgan W. W., 1953, ApJ, 117, 313
Kuiper G. P., 1938, ApJ, 88, 429
Kurucz R. L., 1979, ApJS, 40, 1
Kučinskas A., Hauschildt P. H., Ludwig H. G., Brott I., Vansevičius V., Lindegren L., Tanabé T., Allard F., 2005, A&A, 442, 281
Kučinskas A., Ludwig H. G., Caffau E., Steffen M., 2009, Mem. Soc. Astron. Ital., 80, 723
Laidler V. et al., 2008, Synphot Data User's Guide. STScI, Baltimore
Lee Y. S. et al., 2011, AJ, 141, 90
Lupton R. H., Gunn J. E., Szalay A. S., 1999, AJ, 118, 1406
Lutz T. E., Kelker D. H., 1973, PASP, 85, 573
McCall M. L., 2004, AJ, 128, 2144
McClure R. D., van den Bergh S., 1968, AJ, 73, 313
McWilliam A., 1997, ARA&A, 35, 503
Magic Z., Collet R., Asplund M., Trampedach R., Hayek W., Chiavassa A., Stein R. F., Nordlund Å., 2013, A&A, 557, A26
Maíz Apellániz J., 2006, AJ, 131, 1184
Maíz Apellániz J., 2013, in Guirado J. C., Lara L. M., Quilis V., Gorgas J., eds, Proc. X Scientific Meeting of the Spanish Astronomical Society (SEA), Highlights of Spanish Astrophysics VII, p. 583
Meléndez J., Schuster W. J., Silva J. S., Ramírez I., Casagrande L., Coelho P., 2010, A&A, 522, A98
Milone A. P. et al., 2012, ApJ, 754, L34
Milone A. P. et al., 2014, MNRAS, 439, 1588
Morton D. C., Adams T. F., 1968, ApJ, 151, 611
Mould J. R., Bessell M. S., 1982, ApJ, 262, 142
Mould J. R., Siegel M. J., 1982, PASP, 94, 223
Nataf D. M. et al., 2013, ApJ, 769, 88
Nissen P. E., 1981, A&A, 97, 145
Nissen P. E., Gustafsson B., Edvardsson B., Gilmore G., 1994, A&A, 285, 440
O'Donnell J. E., 1994, ApJ, 422, 158
Oke J. B., Gunn J. E., 1983, ApJ, 266, 713

Oke J. B., Schild R. E., 1970, ApJ, 161, 1015
Önehag A., Gustafsson B., Eriksson K., Edvardsson B., 2009, A&A, 498, 527
Önehag A., Korn A., Gustafsson B., Stempels E., Vandenberg D. A., 2011, A&A, 528, A85
Pinsonneault M. H., An D., Molenda-Żakowicz J., Chaplin W. J., Metcalfe T. S., Bruntt H., 2012, ApJS, 199, 30
Pogson N., 1856, MNRAS, 17, 12
Rajan A. et al., 2011, WFC3 Data Handbook v. 2.1. STScI, Baltimore
Ramírez I. et al., 2012, ApJ, 752, 5
Randich S., Sestito P., Primas F., Pallavicini R., Pasquini L., 2006, A&A, 450, 557
Ridgway S. T., Joyce R. R., White N. M., Wing R. F., 1980, ApJ, 235, 126
Rieke G. H. et al., 2008, AJ, 135, 2245
Roederer I. U., Sneden C., 2011, AJ, 142, 22
Saito R. K. et al., 2012, A&A, 544, A147
Sánchez-Blázquez P. et al., 2006, MNRAS, 371, 703
Sarajedini A. et al., 2007, AJ, 133, 1658
Sarajedini A., Dotter A., Kirkpatrick A., 2009, ApJ, 698, 1872
Sbordone L., Salaris M., Weiss A., Cassisi S., 2011, A&A, 534, A9
Schlafly E. F., Finkbeiner D. P., 2011, ApJ, 737, 103 (SF11)
Schlegel D. J., Finkbeiner D. P., Davis M., 1998, ApJ, 500, 525
Skrutskie M. F. et al., 2006, AJ, 131, 1163
Smith J. A. et al., 2002, AJ, 123, 2121
Stebbins J., Kron G. E., 1957, ApJ, 126, 266
Steffen M., Caffau E., Ludwig H. G., 2013, Mem. Soc. Astron. Ital. Suppl., 24, 37
Stetson P. B., 2005, PASP, 117, 563
Stetson P. B., Hesser J. E., Smecker-Hane T. A., 1998, PASP, 110, 533
Strömgren B., 1966, ARA&A, 4, 433
Tanner J. D., Basu S., Demarque P., 2013, ApJ, 767, 78
Taylor J. R., 1982, An Introduction to Error Analysis. The Study of Uncertainties in Physical Measurements. Oxford Univ. Press, Oxford
Tinsley B. M., 1979, ApJ, 229, 1046
Tokunaga A. T., Vacca W. D., 2005, PASP, 117, 421
Tolstoy E., Hill V., Tosi M., 2009, ARA&A, 47, 371
Torres G., 2010, AJ, 140, 1158
Tremblay P. E., Ludwig H. G., Freytag B., Steffen M., Caffau E., 2013, A&A, 557, A7
Tucker D. L. et al., 2006, Astron. Nachr., 327, 821
VandenBerg D. A., Clem J. L., 2003, AJ, 126, 778
VandenBerg D. A., Casagrande L., Stetson P. B., 2010, AJ, 140, 1020
VandenBerg D. A., Bergbusch P. A., Dotter A., Ferguson J. W., Michaud G., Richer J., Proffitt C. R., 2012, ApJ, 755, 15
VandenBerg D. A., Brogaard K., Leaman R., Casagrande L., 2013, ApJ, 775, 134
VandenBerg D. A., Bergbusch P. A., Ferguson J. W., Edvardsson B., 2014, ApJ, submitted
Wing R. F., 1967, PhD thesis, Univ. California
Worthey G., Faber S. M., Gonzalez J. J., Burstein D., 1994, ApJS, 94, 687
Yanny B. et al., 2009, AJ, 137, 4377
Yong D., Grundahl F., Johnson J. A., Asplund M., 2008, ApJ, 684, 1159

APPENDIX A: INTERPOLATION ROUTINES

The transformations described in this paper and the codes (in FORTRAN) that are needed to tabulate, and interpolate in the BCs for the filters and reddenings of interest are contained in the two files BCtables.tar.gz and BCcodes.tar.gz, respectively. A detailed explanation of their content (and use) is provided in a README file, an excerpt of which is shown in Fig. A1. All these files may be obtained from CDS.

Before describing their contents, a few general remarks are in order. Although the MARCS model atmospheres and synthetic spectra were computed for $-5.0 \leq$ [Fe/H] $\leq +1.0$, $-0.5 \leq \log g \leq 5.5$, $2500 \leq T_{\mathrm{eff}} \leq 8000$ K, and $-0.4 \leq$ [α/Fe] $\leq +0.4$, the

```
This file provides a detailed explanation of the content of BCtables.tar.gz and
BCcodes.tar.gz, along with some details concerning the execution of their
various programs. A quick step-by-step set of instructions
(UNIX/Linux-oriented) is contained in the file INSTRUCTIONS.txt.

The BCtables.tar.gz file contains the following folders, each of which
contains many sub-directories:
1) alpha_m04   2) alpha_p00   3) alpha_p04   4) alpha_std

The BCcodes.tar.gz file contains the following Fortran computer programs:
1) getinputbcs.for  ... code to retrieve BC data for several fixed E(B-V) values
2) getbctable.for   ... code to generate BC transformation tables for any E(B-V)
3) gettestbcs.for   ... code to retrieve original MARCS data (see below)
4) chkbctable.for   ... verification program (see below)
5) bcutil.for       ... subroutines to interpolate in BC transformation tables
6) colstar.for      ... program to illustrate the use of bcinterp.for
7) bcstars.for      ... code to generate BCs for stars of known Teff,logg,[Fe/H]

In addition, BCcodes.tar.gz also contains the following files:
8) selectbc.data    ... to select photometric systems and MARCS models to use
9) input.sample     ... an example of input file for bcstars.for
10)bcgo             ... an executable file to compile, link and run bcstars.for
```

Figure A1. Excerpt of the README file provided with our package.

coverage of parameter space is not complete. For instance, there are no model atmospheres at low gravities and high temperatures (which would be of limited usefulness, anyway), and relatively few computations at the lowest temperatures, gravities, and metallicities, or at $\log g = 5.5$. Moreover, the number of $T_{\rm eff}$ values for which model atmospheres were generated varies with $\log g$, [Fe/H], and [α/Fe]. To deal with this non-uniformity, which obviously presents some challenges for the setting up of interpolation tables, cubic splines were used whenever possible to determine the transformations, which consist of BCs for each filter bandpass that we have considered, when model atmospheres were lacking at gravities and temperatures in the middle of their respective ranges. Linear or three-point extrapolations were also made, as needed, to 'fill in' missing BC entries located near the upper and lower limits of the dependent variables.

In order to minimize the number of extrapolations, while maximizing the size of the transformation tables, the decision was made to restrict the latter to the ranges in gravity and temperature shown in Fig. A2 (the region enclosed by the dashed lines). Victoria-Regina isochrones (VandenBerg et al. 2014) for [Fe/H] $= -2.4$ and $+0.4$, which include masses as low as $0.12\,{\rm M}_\odot$ and extend to the RGB tip, have been included in this plot simply to illustrate where such models are located in this diagram. In this figure, the grid values of $\log g$ and $T_{\rm eff}$ are indicated by the intersection of the dotted grey lines, and it is for these values that BCs are provided. (Tables of exactly the same dimensions have been created for all of the grid values of [Fe/H] and [α/Fe].) Thus, no data are provided for $T_{\rm eff} < 2600$ K, while BCs for $\log g = 5.5$ are given only for $5000 \leq T_{\rm eff} \leq 2600$ K, etc. Perhaps, the most important limitation of the transformation tables is that they can be used only for $T_{\rm eff} \leq 8000$ K, which is a consequence of the fact that MARCS model atmospheres were not computed for higher temperatures. As a result, they cannot be used for, e.g. hot MS or blue horizontal-branch stars – but hopefully an extension of the tables to higher temperatures will be made at some future date.

Once BCtables.tar.gz has been retrieved from CDS, it would be prudent to open it in a separate directory as it contains a fairly extensive set of subdirectories (each containing the BCs for a specific photometric system). BCcodes.tar.gz, which contains the software that manipulates the transformation data, should be opened in the same 'home' directory because the computer programs assume
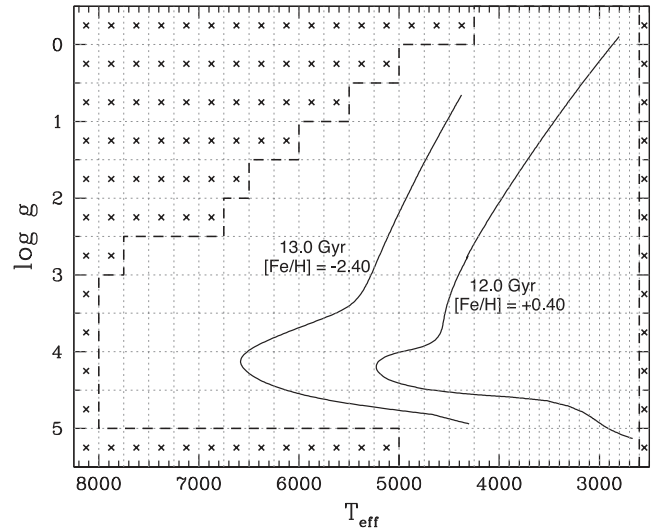

Figure A2. BCs are given for $T_{\rm eff}$ and $\log g$ values within the region enclosed by the dashed lines. (Tables of the same dimensions are provided for each of the grid values of [Fe/H] and [α/Fe], which vary from -4.0 to $+1.0$ and -0.4 to $+0.4$ (for a subset of the [Fe/H] values), respectively (see the text). Isochrones (from VandenBerg et al. 2014) have been plotted to show that the transformations provide sufficient temperature and gravity coverage for stellar models over a wide range in mass ($\gtrsim 0.12\,{\rm M}_\odot$) and evolutionary state.

a particular directory structure for the data files and they will not execute properly unless that structure is in place. Their execution is controlled by the included `selectbc.data` file, a sample of which is shown in Fig. A3. It essentially provides a menu (the information given below the dashed line) that enables the user to select up to five filters for which a table of BCs will be created for subsequent interpolations (so as to, e.g. transform stellar models from the theoretical plane to various CMDs of interest). The main advantage of tabulating BCs, instead of colours, is that the former is a much more compact way of presenting the transformations. For instance, from five BCs for the Johnson–Cousins $UBV(RI)_C$ system, 10 different colour indices ($U - B$, $U - V$, ... $B - V$, ... $R_C - I_C$) can be derived. (Synthetic absolute magnitudes can be calculated from $M_\zeta = M_{\rm bol} - BC_\zeta$ for the ζth filter, and colours may be evaluated from either $\zeta - \eta = M_\zeta - M_\eta$ or $\zeta - \eta = BC_\eta - BC_\zeta$, where ζ represents a bluer bandpass than η.)

The integer on the first line of `selectbc.data` chooses among the four possible variations of [α/Fe] with [Fe/H] for which BC transformations are available. If `ialf = 1`, the so-called standard variation is selected: this assumes [α/Fe] $= +0.4$ for $-4.0 \leq$ [Fe/H] ≤ -1.0, [α/Fe] $= 0.0$ for $0.0 \leq$ [Fe/H] $\leq +1.0$, and [α/Fe] $= -0.4$ for $-1.0 <$ [Fe/H] < 0.0. (Note that BCs are not provided for [Fe/H] < -4.0, even though some MARCS model atmospheres were computed for [Fe/H] $= -5.0$. There were simply too few of the latter cases to cover the adopted ranges in $\log g$ and $T_{\rm eff}$ without having to carry out excessive numbers of extrapolations.) Setting `ialf = 2`, 3, or 4 will result in the retrieval of the BCs for, in turn, [α/Fe] $= +0.4$ for $-2.5 \leq$ [Fe/H] $\leq +0.5$, [α/Fe] $= 0.0$ for $-2.50 \leq$ [Fe/H] $\leq +1.0$, or [α/Fe] $= -0.4$ for $-2.0 \leq$ [Fe/H] $\leq +1.0$.

The second line of `selectbc.data` defines `nfil`, which can have a maximum value of 5. In many applications, the magnitude on the y-axis of a CMD is also used to compute the colour on the x-axis, as in the case of a ($B - V$, V)-diagram; in which case, `ialf` would be set to a value of 2. However, `nfil =5` would be the natural choice for observations obtained in, e.g. the *ugriz* system.

```
2  = ialf (= [alpha/Fe] variation: select from choices listed below)
4  = nfil (= number of filter bandpasses to be considered; maximum = 5)
7 36  =  photometric system and filter (select from menu below)
7 37  =  photometric system and filter (select from menu below)
7 39  =  photometric system and filter (select from menu below)
1  1  =  photometric system and filter (select from menu below)
1  3  =  photometric system and filter (select from menu below)
--------------------------------------------------------------------------------

   ialf:  1: "standard variation" of [alpha/Fe] with [Fe/H]
          2: [alpha/Fe] = +0.4  (for [Fe/H] from -2.5 to +0.5, inclusive)
          3: [alpha/Fe] = +0.0  (for [Fe/H] from -2.5 to +1.0, inclusive)
          4: [alpha/Fe] = -0.4  (for [Fe/H] from -2.0 to +1.0, inclusive)

Photometric system                  Filters

   1 = 2mass         1 = J           2 = H           3 = K_s

                     4 = acs_f435w   5 = acs_f475w   6 = acs_f555w
                     7 = acs_f606w   8 = acs_f814w   9 = acs_f218w
   2 = hst_ab       10 = wfc3_f225w 11 = wfc3_f275w 12 = wfc3_f336w
   3 = hst_st       13 = wfc3_f350lp 14 = wfc3_f390m 15 = wfc3_f390w
   4 = hst_vega     16 = wfc3_f438w 17 = wfc3_f475w 18 = wfc3_f547m
                    19 = wfc3_f555w 20 = wfc3_f606w 21 = wfc3_f625w
                    22 = wfc3_f775w 23 = wfc3_f814w 24 = wfc3_f850lp
                    25 = wfc3ir_f98m 26 = wfc3ir_f110w 27 = wfc3ir_f125w
                    28 = wfc3ir_f140w 29 = wfc3ir_f160w

   5 = sdss         30 = u          31 = g          32 = r
                    33 = i          34 = z

   6 = ubvri12      35 = U          36 = B          37 = V
                    38 = R_C        39 = I_C

   7 = ubvri90      40 = UX         41 = BX         36 = B
                    37 = V          38 = R_C        39 = I_C
```

Figure A3. A sample `selectbc.data` file: it is used to choose among four possible variations of [α/Fe] with [Fe/H] (via the parameter `ialf`), to select the number of filters for which BC transformations are sought (`nfil`), and to identify the particular photometric system(s) and filter(s) of interest (using lines 4–7). The possible options are listed below the horizontal dashed line.

The next 4–7 lines specify the photometric system(s) and filters of choice. In the example given in Fig. A3, the 1990 calibration (named `ubvri90`, see Section 2.9) of the *B*, *V*, and I_C filters, along with the 2MASS K_S filter, have been selected. (The 7*th* line, which specifies the integers 1 and 3, will not be read in this case because `nfil = 4`.) The photometric systems and filters can be identified in any order.

Once the parameters in `selectbc.data` have been set, two programs must be executed in order to obtain the desired BC transformation tables. The first one that needs to be compiled and executed is `getinputbcs.for`. Because reddening-corrected BC values have been derived for $E(B − V) = 0.00$ to 0.72, in steps of 0.02, the user can request transformations for any reddening within this range. However, rather than storing such a large data set, only the tables for $E(B − V) = 0.00, 0.12, 0.24, \ldots 0.72$ have been retained. We found that spline interpolations in tables for these seven reddenings were able to reproduce the reddening-adjusted transformations in the full set of tables to within 0.001 mag, independently of the selected filter. Consequently, the purpose of `getinputbcs.for` is to retrieve from the appropriate subdirectories the BCs for $0.0 \le E(B − V) \le 0.72$, in steps of 0.12 mag. These data are placed in the seven files that have been given the names `inputbc_r00.data`, `inputbc_r12.data`, etc. (These files are rewritten each time `getinputbcs` is executed.)

The next step is to compile and execute `getbctable.for`, which prompts the user for a value of $E(B − V)$ and then interpolates in the `inputbc_*.data` files to produce the requested BC transformations for that choice of the reddening. Since the ranges in [Fe/H] are different for the cases that are specified by the param-

```
Tables of Bolometric Corrections Derived from the 2008 MARCS model atmospheres
31 Teffs          12 log gs         10 [Fe/H]s      4 BC values    E(B-V) = 0.125
2600. 2700. 2800. 2900. 3000. 3100. 3200. 3300. 3400. 3500. 3600. 3700. 3800.
3900. 4000. 4250. 4500. 4750. 5000. 5250. 5500. 5750. 6000. 6250. 6500. 6750.
7000. 7250. 7500. 7750. 8000.
0.0 0.5 1.0 1.5 2.0 2.5 3.0 3.5 4.0 4.5 5.0 5.5
 19  20  21  22  24  30  31  31  31  31  31  19
[Fe/H] = -2.50 [alpha/Fe] = 0.40 BC value =  B       ubvri90
-6.2473 -6.0066 -5.8529 -5.6624 -5.4182 -5.2072 -5.0969 -5.0281 -4.9130 -4.7249
-4.5007 -4.2521 -3.9975 -3.7512 -3.5101 -2.9415 -2.4276 -2.0044 -1.6578
-5.9263 -5.5948 -5.3461 -5.1364 -4.9572 -4.8057 -4.6742 -4.5486 -4.4147 -4.2631
-4.0875 -3.8844 -3.6587 -3.4294 -3.2105 -2.7133 -2.2744 -1.9046 -1.6103 -1.3838
-5.7139 -5.3340 -5.0288 -4.7922 -4.6194 -4.4767 -4.3328 -4.1871 -4.0439 -3.9021
-3.7486 -3.5765 -3.3802 -3.1712 -2.9713 -2.5303 -2.1517 -1.8283 -1.5730 -1.3744
-1.2132
                        .
                        .
                        .
-4.9171 -4.6908 -4.4853 -4.2907 -4.1072 -3.9323 -3.7627 -3.5956 -3.4290 -3.2639
-3.1010 -2.9422 -2.7892 -2.6434 -2.5078 -2.1968 -1.9451 -1.7380 -1.5671
[Fe/H] = -2.00 [alpha/Fe] = 0.40 BC value =  B       ubvri90
-6.3294 -6.0398 -5.7994 -5.5961 -5.4189 -5.2534 -5.0865 -4.9085 -4.7184 -4.5169
-4.2988 -4.0642 -3.8221 -3.5885 -3.3583 -2.8647 -2.4207 -2.0252 -1.7015
-5.9469 -5.6175 -5.3456 -5.1241 -4.9394 -4.7770 -4.6240 -4.4676 -4.3045 -4.1321
-3.9445 -3.7380 -3.5161 -3.2964 -3.0916 -2.6442 -2.2591 -1.9201 -1.6360 -1.4095
-5.6716 -5.2983 -5.0016 -4.7825 -4.5830 -4.4128 -4.2615 -4.1167 -3.9710 -3.8203
-3.6595 -3.4828 -3.2864 -3.0812 -2.8877 -2.4749 -2.1342 -1.8396 -1.5888 -1.3859
-1.2189
                        .
                        .
```

Figure A4. The first ∼25 lines of the output file that is produced if `getinputbcs` and `getbctable` are executed when the values of the initializing parameters in `selectbc.data` are set to the values shown in the previous figure. As indicated in the second line, these transformations assume $E(B − V) = 0.125$, which is the reddening value that was entered in response to a prompt that is issued by `getbctable`.

eter `ialf` (see above), the output file generated by `getbctable` is given the name `bc_std.data` if `ialf = 1`, `bc_p04.data` if `ialf = 2`, `bc_p00.data` if `ialf = 3`, or `bc_m04.data` if `ialf = 4`. Perhaps, the main reason for doing this is to facilitate interpolations in the resultant transformations for arbitrary values of [α/Fe] within the range $−0.4 \le [α/Fe] \le +0.4$. (To perform such interpolations, it is clearly necessary to cycle through the above procedure in order to create the respective `bc_*.data` files corresponding to `ialf = 2, 3,` and 4.) Note that `getinputbcs` and `getbctable` are completely self-contained; i.e. all file assignments are done internally. In summary, to obtain reddening-adjusted BC transformations for up to five different filters, one simply sets the parameters in `selectbc.data` to the desired values, and then executes `getinputbcs` and `getbctable`.

The output data files so obtained have been organized in a straightforward way. Fig. A4 reproduces the beginning of the `bc_p04.data` file that would be created using the example of `selectbc.data` given in the previous figure. The first (title) line is included primarily to reinforce the fact that the quantities in the tables are BCs (not colours). The second line specifies the number of T_{eff}, gravities, [Fe/H] values, and BCs, as well as the reddening value that was entered when prompted for it by `getbctable`. The next four lines list the grid values of T_{eff} and log *g*, while the following (7*th*) line specifies how many BC values, beginning with the first entry at 2600 K, are included in the table at each log *g* value. For example, the minimum gravity in this table is log *g* = 0.0, and according to the first entry on the seventh line, BC transformations are provided for the first 19 values of T_{eff} (i.e. up to 5000 K), which is consistent with what is shown in Fig. A2. The seventh line thus helps to describe the irregular shape of the region in T_{eff}, log *g* space where interpolations are permitted.

The rest of the sample `bc_p04.data` file lists, in the form of mini-tables, BCs in the order of increasing [Fe/H], and within each

table, they are organized in rows for the grid values of log g, with a maximum of 10 numbers per row. Hence, the 19 BC values at log $g = 0.0$, in the order of increasing T_{eff}, are contained in the two rows immediately after the header line that gives the values of [Fe/H] and [α/Fe] which are applicable to the BC data that follow. All of the transformations for a given filter, which is also identified in the mini-table header lines are grouped together. Thus, all of the transformations for the `ubvri90` *B* filter are listed before all of those for the *V* filter (which are likewise organized in the direction of increasing [Fe/H]), etc.

In addition to subroutines (such as `getbcs_p04.for`) that perform interpolations in the BC tables, `BCcodes.tar.gz` contains programs that can be used to verify that everything is working correctly. To be more specific, `gettestbcs.for` retrieves from the appropriate subdirectories, the original MARCS transformations that were used in the construction of the interpolation tables (for one of six possible values of $E(B − V)$; namely, 0.0, 0.08, 0.14, 0.28, 0.44, or 0.56). These data are stored in files with names like `sph00.data` or `ppl40.data`, where the prefixes `sph` and `ppl` indicate that the data are based on 'spherical' or 'plane-parallel' model atmospheres, respectively, and the two digits indicate the log g value (e.g. `00` implies 0.0 whereas `40` implies 4.0; log $g = −0.5$ is coded as `m05`). These values of $E(B − V)$ were chosen so as to be offset by different amounts from the values (0.0, 0.12, 0.24, 0.36, . . .) used in the spline fits.

The second of three steps in the verification process is to run `getbctable` for the same value of the reddening. In the final step, which requires the execution of `chkbctable.for`, the [Fe/H], T_{eff}, and log g values listed in the `sph*.data` and `ppl*.data` files are used to obtain BC values, by interpolating in the output file from `getbctable`: these are then compared with the values in the original MARCS tables (i.e. `sph*.data`, etc.). In our experience, the differences between the interpolated and tabulated BCs are always <0.001 mag: they tend to be the largest for blue and UV bandpasses. Differences will be exactly 0.0 only when the BCs for $E(B − V) = 0.0$ are selected by `gettestbcs` given that exactly the same data are employed in the construction of the splines. A short program, with results, is also included in the package to illustrate how to perform interpolations in the tables produced by `getbctable`. As already pointed out, a detailed explanation of these auxiliary codes is contained in a README file that is also provided.

Finally, it is worth mentioning that the extinction coefficients (and reddening values) that apply to reddened stars of different spectral types may be easily calculated using our interpolation routines. Consider, for instance, an old, moderately metal-poor ([Fe/H] = −0.8, [α/Fe] = +0.4), TO star (T_{eff} = 5950 K, log g = 4.2) that is affected by a nominal reddening $E(B − V) = 0.6$. On the assumption of the canonical extinction law, $R_V = 3.1$, the following BCs are obtained in a number of selected bands: $BC_B = −3.03$, $BC_V = −1.97$, $BC_g = −2.54$, $BC_r = −1.58$. If that star were unreddened, the values of the same BCs would be: $BC_B = −0.61$, $BC_V = −0.10$, $BC_g = −0.30$, and $BC_r = 0.04$. It thus follows that, at the TO, $E(B − V) = (−1.97 + 3.03) − (−0.10 + 0.61) = 0.55$ and $E(g − r) = (−1.58 + 2.54) − (0.04 + 0.30) = 0.62$, with extinction coefficients $R_B = \frac{3.03−0.61}{0.55} = 4.40$, $R_V = \frac{1.97−0.10}{0.55} = 3.40$, $R_g = \frac{2.54−0.30}{0.55} = 4.07$, and $R_r = \frac{1.58+0.04}{0.55} = 2.95$. Note, in particular, that the difference $R_B − R_V$ is exactly 1.0 *because* the extinction coefficients were calculated assuming the value of $E(B − V)$ that applies to the star in question.

This difference would be <1 if the $E(B − V)$ value appropriate to early-type stars is adopted – which is the usual conven-

tion for reddening determinations that are reported in the literature. Returning to the example considered in the previous paragraph, $R_B = \frac{3.03−0.61}{0.6} = 4.03$ and $R_V = \frac{1.97−0.10}{0.6} = 3.12$, with the result that $R_B − R_V = 0.91$ and $E(B − V) = (0.91)(0.6) = 0.55$. Reinforcing the point already made in Section 5 (also see Bessell et al. 1998), these calculations show that the $E(B − V)$ value produced by a given amount of dust will be significantly less for a 5950 K (late F-type) TO star than for early O- and B-type stars. Similarly, colour excess ratios will scale according to spectral type since, for filters ζ and η, the difference $R_\zeta − R_\eta$ is equal to $E(\zeta − \eta)/E(B − V)$, where the denominator of this term is the nominal reddening. Clearly, to correct colours (equation 20) and magnitudes (equation 21) for the effects of interstellar extinction, one should use *either* 0.55 and (3.4)(0.55) *or* (0.60)(0.91) and (3.12)(0.60), respectively, in the case of the present example.

In comparisons of isochrones with observed CMDs, it is traditional to apply constant offsets to the observed magnitudes and/or colours (depending on whether an apparent or true distance modulus is assumed) to account for the effects of foreground gas and dust. This is much simpler than correcting the observations (or, more likely, the isochrones) on a point-by-point basis prior to fitting the models to the data, and indeed, there is no reason to abandon this practice if, e.g. the main goal of the work is to derive the TO age(s). (Recall the discussion in Section 5 concerning Fig. 18, which showed that, even when the reddening is high, the two approaches lead to no more than minor differences along the RGB and the lower MS.) Since published R_ζ values are generally based on hot stars (e.g. Vega, in the case of McCall 2004), we have calculated the extinction coefficients relevant to TO stars (log g = 4.1), 5250 ≤ T_{eff} ≤ 7000 K (in 250 K increments), and −2.0 ≤ [Fe/H] ≤ +0.25 (at the specific values adopted in the MARCS library). (This involves nothing more than evaluating A_ζ from the difference in the BCs assuming two nominal reddening values, which we choose to be $E(B − V) = 0.0$ on the one hand, and $E(B − V) = 0.10$, on the other, and then dividing by 0.10.) Variations in [α/Fe] were also considered, but the dependence of R_ζ on this abundance parameter was found to be sufficiently weak that it could be ignored: the results for [α/Fe] = −0.4, 0.0, and +0.4 were simply taken to be alternative determinations for the associated [Fe/H] value.

Table A1 lists, for the majority of the filters considered in this study, the mean extinction coefficients so obtained $< R_\zeta >$, along with a least-squares fit to the data assuming a functional dependence[15] $R_\zeta = a_0 + T_4(a_1 + a_2T_4 + a_3[Fe/H])$, where $T_4 = 10^{−4}T_{eff}$. With relatively few exceptions, $\langle R_\zeta \rangle$ reproduces the values of the extinction coefficients that were computed for the aforementioned values of log g, T_{eff}, [Fe/H], and [α/Fe] to within 1 per cent. The largest residuals, amounting to ∼1.6 per cent, were found for the *B*, *g*, and approximately equivalent *HST* filters. Both the maximum residuals and the rms deviations, which are typically one-third as large, are reduced by about a factor of 5 if the least-squares fit to R_ζ is adopted instead of the mean value. Only in the case of the *F218W*, *F225W*, *F275W*, and *F350LP* filters, it was not possible to obtain a good fit to the actual values of R_ζ; consequently, they have been omitted from this table. (The mean values were likewise very poor approximations, undoubtedly due to the strong T_{eff} dependence of the BCs in these four filters.) In any case,

---

[15] Users are warned not to extrapolate these relations outside of the range of their applicability. Such caution is advisable even though the dependence of the extinction coefficients on T_{eff} is usually less dramatic above 10 000 K – as we have found using ATLAS9 models.

Table A1. Values of R_ζ relevant to TO stars with $T_{eff} \lesssim 7000\,\text{K}^a$. Notice that for a *nominal* $E(B - V)$, the excess in any given $\zeta - \eta$ colour is $E(\zeta - \eta) = (R_\zeta - R_\eta)E(B - V)$, and the attenuation for a magnitude m_ζ is $R_\zeta E(B - V)$. See also discussion in the text.

| Filter | $\langle R_\zeta \rangle$ | $R_\zeta = a_0 + T_4\,(a_1 + a_2\,T_4) + a_3\,[\text{Fe/H}]$ | | | | Filter | $<R_\zeta>$ | $R_\zeta = a_0 + T_4\,(a_1 + a_2\,T_4) + a_3\,[\text{Fe/H}]$ | | | |
		a_0	a_1	a_2	a_3			a_0	a_1	a_2	a_3
					2MASS						
J	0.899	0.9095	−0.0526	0.0583	–	H	0.567	0.5611	0.0176	−0.0115	–
K_S	0.366	0.3667	−0.0026	0.0021	–						
					ACS						
$F435W$	4.106	3.4929	1.7330	−1.2071	−0.0135	$F475W$	3.720	3.1735	1.4136	−0.8569	−0.0078
$F555W$	3.217	3.0197	0.4900	−0.2738	−0.0018	$F606W$	2.876	2.5200	0.8308	−0.4074	−0.0018
$F814W$	1.884	1.7763	0.2522	−0.1227	–						
					WFC3^b						
$F336W$	5.148	4.9002	0.6329	−0.3806	−0.0062	$F390M$	4.503	4.3391	0.5133	−0.4007	−0.0015
$F390W$	4.432	3.6722	2.3798	−1.8697	−0.0165	$F438W$	4.135	3.8431	0.8230	−0.5695	−0.0055
$F475W$	3.698	3.1588	1.4014	−0.8529	−0.0071	$F547M$	3.140	3.0439	0.2472	−0.1483	−0.0015
$F555W$	3.274	2.8862	0.9399	−0.5000	−0.0023	$F606W$	2.894	2.5345	0.8514	−0.4306	−0.0020
$F625W$	2.678	2.5954	0.1656	−0.0481	–	$F775W$	2.049	2.0174	0.0527	−0.0003	–
$F814W$	1.897	1.8027	0.2058	−0.0818	–	$F850LP$	1.457	1.3997	0.1673	−0.1192	–
$F098M$	1.290	1.2709	0.0432	−0.0193	–	$F110W$	1.047	0.9272	0.2848	−0.1428	–
$F125W$	0.891	0.8675	0.0394	−0.0027	–	$F140W$	0.753	0.7180	0.0754	−0.0290	–
$F160W$	0.634	0.6196	0.0301	−0.0100	–						
					SDSS						
u	4.862	4.5725	0.9248	−0.7397	−0.0051	g	3.762	3.2679	1.2843	−0.7840	−0.0076
r	2.704	2.6623	0.0691	−0.0017	–	i	2.120	2.0927	0.0464	−0.0019	–
z	1.528	1.4713	0.1576	−0.1052	–						
					ubvri12						
U	4.801	4.3796	1.3861	−1.1400	−0.0065	B	4.046	3.3504	1.8900	−1.2437	−0.0143
V	3.122	2.9364	0.4604	−0.2568	−0.0022	R_C	2.552	2.4248	0.2672	−0.0932	–
I_C	1.902	1.8662	0.0657	−0.0098	–						
					ubvri90						
UX	4.814	4.3241	1.6005	−1.3063	−0.0073	BX	4.032	3.2999	2.0123	−1.3425	−0.0140
B	4.049	3.3155	2.0119	−1.3400	−0.0145	V	3.129	2.9256	0.5205	−0.3078	−0.0022
R_C	2.558	2.4203	0.3009	−0.1220	–	I_C	1.885	1.8459	0.0741	−0.0151	–

^{a} Based on the differences in the BCs for $E(B - V) = 0.0$ and 0.10, assuming $\log g = 4.1$, $5250 \le T_{eff} \le 7000\,\text{K}$, $-2.0 \le [\text{Fe/H}] \le +0.25$, and $-0.4 \le [\alpha/\text{Fe}] \le +0.4$. In the fitting equation for R_ζ, $T_4 = 10^{-4}\,T_{eff}$. ^{b} Results are not provided for the $F218W$, $F225W$, $F275W$, and $F350LP$ filters because of their strong dependence on T_{eff}.

Table A1 provides two ways of determining approximate (but still quite accurate) values of R_ζ that can be used to evaluate the colour excess ratio for any of the filters that are listed. Importantly, such ratios involve the *nominal* reddening given that all of our R_ζ results are based on the standard extinction law, $R_V = 3.1$.

APPENDIX B: BIAS IN A NON-LINEAR TRANSFORMATION

Every time a non-linear transformation is applied to a variable that is subject to random errors (in this context e.g. an observed quantity with a Gaussian probability distribution function; PDF) a skewed PDF arises as a consequence of the transformation. In this case, the expectation value differs from the mode and the difference between the two introduces a bias. This traces directly back to a better-known example, such as the bias between parallaxes and distances (e.g. Lutz & Kelker 1973; Casagrande et al. 2007).

Let us consider the case of transforming a magnitude m into a heterochromatic flux $\mathcal{F}$, which (from equation 1) involves the following non-linear relation

$$\mathcal{F} = \alpha\,10^{-0.4\,m}, \tag{B1}$$

where α is a constant that incorporates all of the details concerning the absolute calibration and zero-point of the photometric system under consideration.

Assuming a Gaussian distribution for the errors around m (as obtained e.g. by averaging different independent measurements)

$$f(\tilde{m}) = \frac{1}{\sqrt{2\pi}\sigma}\,e^{-\frac{(\tilde{m}-m)^2}{2\sigma^2}}, \tag{B2}$$

the expectation value for the flux $\mathcal{F}$ is

$$E\left[\mathcal{F}|m\right] = \int_{-\infty}^{+\infty} \mathcal{F}(\tilde{m})\,f(\tilde{m})\,d\tilde{m}$$

$$= \frac{\alpha}{\sqrt{2\pi}\sigma}\,10^{-0.4\,m}\int_{-\infty}^{+\infty} 10^{-0.4\,u}\,e^{-\frac{u^2}{2\sigma^2}}\,du$$

$$= \alpha\,10^{-0.4\,m}\,e^{0.08\,\sigma^2\,\ln^2(10)}, \tag{B3}$$

where $u = \tilde{m} - m$. The amplitude of the bias can be immediately estimated by comparing equations (B3) and (B1), or in fractional terms

$$\frac{E\left[\mathcal{F}|m\right] - \mathcal{F}}{\mathcal{F}} = e^{0.08\,\sigma^2\,\ln^2(10)} - 1. \tag{B4}$$

Fortunately, this difference is negligible in most investigations, when uncertainties are of the order of few hundredths of a magnitude, although it quickly rises from 1 per cent at $\sigma \simeq 0.2$ mag to 10 per cent at $\sigma \simeq 0.7$ mag.

Notice that the opposite bias is also present. In fact, in the above example we have assumed that the errors arise as a consequence of

averaging a number of independent measurements. In reality, when measuring magnitudes, several steps are involved, which essentially consist of transforming number counts into fluxes (for CCD detectors), and fluxes into magnitudes, which then are corrected for atmospheric extinction (in the case of ground-based observations) and standardized using photometric equations (e.g. Harris, Fitzgerald & Reed 1981). Assuming that the uncertainty of the photometric equations is small, which is usually the case if a sufficient number of standards has been observed spanning different colours and airmasses, with decreasing signal to noise, the main uncertainty of a magnitude stems from its flux measurement. We also assume that the uncertainty in flux measurements is Gaussian, which is appropriate since a Poisson distribution is well approximated by a Gaussian after relatively few counts (e.g. Taylor 1982).

For objects with high signal to noise, the flux uncertainty has a narrow Gaussian peak, which transforms to negligible uncertainty in magnitude. However, as the signal to noise decreases, the uncertainty in the flux broadens (and other sources of random errors can also become important; e.g. Howell 1989). As before, if we know the flux $\mathcal{F}$, we can compute the expectation value for a magnitude using the full PDF

$$
\begin{aligned}
E[m|\mathcal{F}] &= \int_{-\infty}^{+\infty} m(\tilde{\mathcal{F}}) f(\tilde{\mathcal{F}}) \mathrm{d}\tilde{\mathcal{F}} \\
&= -\frac{2.5}{\sqrt{2\pi}\sigma} \int_{-\infty}^{+\infty} \log\left(\frac{\tilde{\mathcal{F}}}{\alpha}\right) \mathrm{e}^{-\frac{(\tilde{\mathcal{F}}-\mathcal{F})^2}{2\sigma^2}} \mathrm{d}\tilde{\mathcal{F}} \\
&= 2.5\log(\alpha) - \frac{2.5}{\sqrt{2\pi}\sigma} \int_{-\infty}^{+\infty} \log(\tilde{\mathcal{F}}) \mathrm{e}^{-\frac{u^2}{2\sigma^2}} \mathrm{d}u,
\end{aligned}
\tag{B5}
$$

where $u = \tilde{\mathcal{F}} - \mathcal{F}$, and expanding $\log(\tilde{\mathcal{F}})$ around the maximum of $-u^2$, we obtain

$$
\begin{aligned}
E[m|\mathcal{F}] =\ & 2.5\log(\alpha) - \frac{2.5}{\sqrt{2\pi}\sigma} \int_{-\infty}^{+\infty} \Bigg[\log(\mathcal{F}) \\
&+ 5\log(\mathrm{e}) \sum_{n=1}^{\infty} \frac{(-1)^{n+1}}{n} \left(\frac{u}{\mathcal{F}}\right)^n \Bigg] \mathrm{e}^{-\frac{u^2}{2\sigma^2}} \mathrm{d}u \\
=\ & -2.5\log\left(\frac{\mathcal{F}}{\alpha}\right) - 2.5 \frac{5\log(\mathrm{e})}{\sqrt{2\pi}\sigma} \\
&\times \int_{-\infty}^{+\infty} \left[\sum_{n=1}^{\infty} \frac{(-1)^{n+1}}{n} \left(\frac{u}{\mathcal{F}}\right)^n \right] \mathrm{e}^{-\frac{u^2}{2\sigma^2}} \mathrm{d}u,
\end{aligned}
\tag{B6}
$$

whose solution is not trivial, especially when large errors will formally return negative fluxes. Nevertheless, for errors up to $\simeq 30$ per cent in flux (i.e. the limit where no negative flux is found within 3σ), the above expression can be conveniently approximated using the first term of the expansion, thus leading to an estimate of the bias

$$
E[m|\mathcal{F}] + 2.5\log\left(\frac{\mathcal{F}}{\alpha}\right) \simeq 0.6\left(\frac{\sigma}{\mathcal{F}}\right)^2 .
\tag{B7}
$$

Notice that the two biases discussed here, $E[\mathcal{F}|m]$ and $E[m|\mathcal{F}]$ do not cancel each other, but are representative of two approaches typically used for estimating errors. In the first case, the bias in the flux arises if the error in magnitude is obtained by averaging different measurements. In the second, the bias follows from the fact that symmetric errors in the fluxes are asymmetric once transformed into magnitudes. In either case, when publishing photometry, the procedure used to determine the errors should always be described, in particular for the object with the lowest precision (although formally the bias is always present). If this is not done, users should refrain from (or be very cautious in) analysing statistically large samples of poor-quality data, in the hope that average quantities (with formally small uncertainties) will still be useful: severe biases could undermine the mean results so obtained.

SUPPORTING INFORMATION

Additional Supporting Information may be found in the online version of this article:

BCtables.tar.gz
BCcodes.tar.gz
(http://mnras.oxfordjournals.org/lookup/suppl/doi:10.1093/mnras/stu1476/-/DC1).

Please note: Oxford University Press is not responsible for the content or functionality of any supporting materials supplied by the authors. Any queries (other than missing material) should be directed to the corresponding author for the article.

This paper has been typeset from a TeX/LaTeX file prepared by the author.